Transitions to chaos in two-dimensional double-diffusive convection

By EDGAR KNOBLOCH

Department of Physics, University of California, Berkeley, CA 94720, USA

DANIEL R. MOORE

Department of Mathematics, Imperial College, London SW7 2BZ, UK

JURI TOOMRE

Joint Institute for Laboratory Astrophysics and Department of Astrophysical, Planetary and Atmosphere Sciences, University of Colorado, Boulder, CO 80309, USA

AND NIGEL O. WEISS

Department of Applied Mathematics and Theoretical Physics, University of Cambridge, Cambridge CB3 9EW, UK

The partial differential equations governing two-dimensional thermosolutal convection in a Boussinesq fluid with free boundary conditions have been solved numerically in a regime where oscillatory solutions can be found. A systematic study of the transition from nonlinear periodic oscillations to temporal chaos has revealed sequences of period-doubling bifurcations. Overstability occurs if the ratio of the solutal to the thermal diffusivity $\tau < 1$ and the solutal Rayleigh number R_S is sufficiently large. Solutions have been obtained for two representative values of τ. For $\tau = 0.316$, $R_S = 10^4$, symmetrical oscillations undergo a bifurcation to asymmetry, followed by a cascade of period-doubling bifurcations leading to aperiodicity, as the thermal Rayleigh number R_T is increased. At higher values of R_T, the bifurcation sequence is repeated in reverse, restoring simple periodic solutions. As R_T is further increased more period-doubling cascades, followed by chaos, can be identified. Within the chaotic regions there are narrow periodic windows, and multiple branches of oscillatory solutions coexist. Eventually the oscillatory branch ends and only steady solutions can be found. The development of chaos has been investigated for $\tau = 0.1$ by varying R_T for several different values of R_S. When R_S is sufficiently small there are periodic solutions whose period becomes infinite at the end of the oscillatory branch. As R_S is increased, chaos appears in the neighbourhood of these heteroclinic orbits. At higher values of R_S, chaos is found for a broader range in R_T. A truncated fifth-order model suggests that the appearance of chaos is associated with heteroclinic bifurcations.

1. Introduction

The last decade has seen great progress in understanding the complicated dynamics of nonlinear systems. Some of the most striking advances relate to the transition from periodic to aperiodic (or chaotic) oscillations. To describe these results, let us consider a lightly damped system, acted upon by a spring, which oscillates with gradually

decaying amplitude about a stable equilibrium position. Suppose that the spring is opposed by a weak destabilizing force. Nothing significant happens if both forces are in phase but if there is a phase lag between the destabilizing and stabilizing forces the system may be overstable, so that small oscillations grow exponentially with time. Their growth must ultimately be limited by nonlinear effects and periodic finite-amplitude oscillations will typically ensue. If the destabilizing force is gradually increased, these oscillations will increase in amplitude and become more obviously nonlinear. Eventually they may give way to chaotic behaviour. Two important questions then arise: by what route does the transition proceed? and what mechanism is responsible for the appearance of chaos?

There are only a limited number of routes to chaos (Eckmann 1981). Of these, the most likely is by a sequence of bifurcations at each of which the period doubles, forming a cascade with an accumulation point (Lanford 1982). Beyond that point the oscillations are typically aperiodic, though there are narrow windows where periodic behaviour can be recovered. This intricate pattern of bifurcations has been thoroughly investigated for one-dimensional maps (May 1976; Collet & Eckmann 1980) and has been identified in various experiments. Solutions of ordinary differential equations also exhibit period-doubling bifurcations (e.g. Sparrow 1982) and, as we shall see, they can be found for partial differential equations too.

Cascades of period-doubling bifurcations are associated with transitions to chaos but do not in themselves explain why chaos is produced. In simple systems of differential equations chaotic behaviour is typically associated with orbits of infinite period linking one or more saddle points. A trajectory connecting the unstable and stable manifolds of the same saddle point is called a homoclinic orbit; one that connects two different saddle points is called heteroclinic. As a control parameter is increased there may, in certain circumstances, be homoclinic or heteroclinic bifurcations that are responsible for producing chaos (Guckenheimer & Holmes 1983). In the Lorenz system there is a saddle point with real eigenvalues at the origin in phase space, and a symmetrical pair of homoclinic orbits leads first to 'preturbulence' and then to the appearance of a strange attractor (Sparrow 1982). In other systems there is a saddle-focus and the homoclinic orbit emerges on the eigenvector corresponding to a real positive eigenvalue but returns to spiral slowly in. Shil'nikov (1965) showed that such a homoclinic bifurcation could give rise to chaos.

These bifurcations are not just a mathematical curiosity. Experiments on convection in liquid helium (Libchaber & Maurer 1981), mercury (Libchaber, Laroche & Fauve 1982; Libchaber, Fauve & Laroche 1983) and even water (Gollub & Benson 1980; Giglio, Musazzi & Perini 1981) have demonstrated that period doubling occurs in real fluid systems. It follows that it must be possible to find period doubling, followed by chaos, in solutions of the Navier–Stokes equations. In this paper we consider a classic fluid dynamical problem that exhibits oscillatory behaviour – double-diffusive convection – and examine the transition to chaos. Our aim is to analyse the behaviour found in numerical experiments and, by judicious use of simple models, to explain why chaos occurs. This problem provided the first example of period-doubling in solutions of partial differential equations and also shows how chaos is related to a heteroclinic bifurcation. A preliminary account of some of our results was given by Moore *et al.* (1983).

Double-diffusive phenomena have received considerable attention (e.g. Turner 1973; Huppert & Turner 1981). We consider convection in a fluid layer containing a bottom-heavy distribution of a solute, such as salt, that is heated from below. The stabilizing solute gradient acts as a restoring spring, supporting internal gravity

waves, while the thermal stratification provides a destabilizing force. If the solute gradient is sufficiently strong, oscillatory convection can set in even when the mean density decreases upwards (Stern 1960). In order to produce the necessary phase lag between stabilizing and destabilizing forces it is, however, necessary that the thermal diffusivity, κ_T, should be greater than the solutal diffusivity, κ_S. Finite-amplitude oscillations have indeed been found in experiments on thermosolutal convection (Shirtcliffe 1967, 1969) but at larger values of the thermal Rayleigh number R_T oscillatory convection gives way to steady overturning motion, and the system typically breaks up into a series of convective layers separated by diffusive interfaces (e.g. Turner 1968; Huppert & Linden 1979). Oscillatory convection also occurs in several related problems, where motion is driven by the Soret effect (e.g. Schechter, Velarde & Platten 1974; Knobloch 1980) or constrained by the presence of rotation or magnetic fields (e.g. Chandrasekhar 1961; Busse 1978; Proctor & Weiss 1982).

Two-dimensional thermosolutal convection between free boundaries was studied numerically by Veronis (1968) and by Huppert & Moore (1976; see also Huppert 1977); oscillations between rigid boundaries have been reported by Chang, Korpela & Lee (1982). Huppert & Moore observed complex behaviour associated with the transition from oscillatory to steady convection. They found that for large enough values of the solutal Rayleigh number, R_S (which measures the stabilizing effect of the solute gradient), the oscillations underwent a bifurcation to asymmetry (with unequal clockwise and anticlockwise motion) as R_T was increased. For yet larger values of R_S they found aperiodic oscillations, which eventually gave way to steady overturning motion.

In order to ascertain the origin of this behaviour it is useful to begin with simpler systems of nonlinear differential equations. Moore & Spiegel (1966; Baker, Moore & Spiegel 1971) constructed a nonlinear oscillator that served as a model of overstable thermal convection. This third-order system exhibits a transition from periodic to aperiodic oscillations which turns out to be associated with period-doubling bifurcations (Marzec & Spiegel 1980) and the presence of a heteroclinic orbit (Spiegel 1985). Da Costa, Knobloch & Weiss (1981) studied a model of two-dimensional thermosolutal convection, consisting of five ordinary differential equations, that was originally suggested by Veronis (1965). This model is an exact consequence of expanding the partial differential equations to second order in the amplitude of the motion. Thus the linear and small-amplitude behaviour is identical with that of the partial differential equations. In particular, Knobloch & Proctor (1981) showed that, in a range of values of R_S for which the oscillation amplitude remains small, the period of the oscillation tends to infinity with increasing R_T before the oscillations disappear. This behaviour is associated with the appearance of a heteroclinic orbit; thus the branch of oscillatory solutions terminates on a branch of unstable steady solutions in an amplitude–Rayleigh number diagram. Such behaviour has been verified numerically for the fifth-order model. At larger values of R_S the oscillations increase in amplitude and Da Costa *et al.* (1981) found a bifurcation to asymmetry followed by a cascade of period-doubling bifurcations, with aperiodic oscillations beyond the accumulation point. Typically the sequence of bifurcations would then be repeated in reverse forming a 'bubble' (Knobloch & Weiss 1981) before the oscillatory solutions disappeared. A detailed investigation of the analogous fifth-order model of magnetoconvection revealed an intricate sequence of semiperiodic bands interspersed with periodic windows beyond the accumulation point of the initial cascade, and confirmed that the oscillatory branch terminated with a heteroclinic orbit (Knobloch & Weiss 1983; Bernoff 1985). Moreover, the appearance of chaos is associated with

a heteroclinic connection between saddle foci with eigenvalues satisfying Shil'nikov's (1965) inequality. In double-diffusive convection, chaos is apparently caused by heteroclinic bifurcations.

The fifth-order model provides a nice example of the applications of modern bifurcation theory (Guckenheimer & Holmes 1983) and these results encouraged us to seek similar behaviour in solutions of the full partial differential equations. In this paper we present numerical evidence for an initial bifurcation to asymmetry, followed by period-doubling, semiperiodic bands and periodic windows. The bubble structure reappears and is associated with the heteroclinic bifurcation that seems to be responsible for producing chaos. This complicated web could scarcely have been unravelled without prior study of the fifth-order system.

Aperiodic oscillations have been seen in numerical solutions of various systems of partial differential equations, including studies of two- and three-dimensional Rayleigh–Bénard convection (McLaughlin & Orszag 1982; Curry, Herring, Loncaric & Orszag 1984) and of convection in porous media (Schubert & Straus 1982). Such oscillations are readily found in numerical simulations of three-dimensional convection, though the origins of chaos are usually unclear. One route to chaos that has been much discussed is by the breakdown of triply periodic motion, corresponding to the appearance of a strange attractor after three successive Hopf (i.e. oscillatory) bifurcations (Ruelle & Takens 1971; Newhouse, Ruelle & Takens 1978; Eckmann 1981). Although quasi-periodic (i.e. multiply periodic) behaviour with three or more incommensurate frequencies is structurally unstable (Newhouse *et al.* 1978) the perturbations of the system required to produce chaotic motion are apparently very special (Arnol'd 1983) and there are several examples of stable triply or quadruply periodic motion (Gollub & Benson 1980; Grebogi, Ott & Yorke 1983, 1985; Tavakol & Tworkowski 1984 *a, b*). We suspect that transitions to chaos in three-dimensional convection, following one or more Hopf bifurcations, are generally associated with cascades of period-doubling bifurcations (preceded, where necessary, by frequency locking to give a periodic orbit). To locate such a cascade requires a very detailed search and in three-dimensional computations this is difficult to carry out.

In two-dimensional problems it is, however, feasible to conduct an intensive search and to identify both the route to chaos and the mechanism responsible for causing it. The transitions to chaos that we shall describe here all occur by period doubling. With one exception, chaos appears after a single Hopf bifurcation, followed by a cascade of period-doubling bifurcations; in a single case (with rather extreme parameter values) whose accuracy is not yet fully established there are two Hopf bifurcations leading to doubly periodic motion (so that trajectories lie on a two torus in phase space), followed by frequency locking and a period-doubling cascade. These cascades are associated with a global bifurcation that produces a heteroclinic orbit connecting two saddle foci. It can be shown that, under certain conditions, such a bifurcation must be accompanied by infinitely many (possibly coexisting) period-doubling cascades, leading to intervals of chaos (Glendinning & Sparrow 1984; Gaspard, Kapral & Nicolis 1984; Arnéodo *et al.* 1985 *b*). This mechanism, due to Shil'nikov (1965; Guckenheimer & Holmes 1983), is known to operate near certain multiple bifurcations in systems described by partial differential equations (Guckenheimer 1981; Arnéodo *et al.* 1985 *b*). Indeed, it has been demonstrated that this mechanism can generate chaos arbitrarily close to the initial bifurcation for thermosolutal convection in a rotating system (Arnéodo, Coullet & Spiegel 1985 *a*; Arnéodo & Thual 1985).

Our paper is organized as follows. In §2 we survey the whole problem: after

summarizing known analytical and numerical results we present new computations which show that the transition to chaos does indeed take place via a cascade of period-doubling bifurcations; we also indicate how this behaviour relates to the fifth-order model. We then describe, in §3, a detailed investigation of successive bifurcations along the branch of oscillatory solutions. The results are illustrated by projecting trajectories onto suitable phase planes and constructing associated return maps and by obtaining frequency power spectra. We have located several bubbles with chaotic behaviour interspersed with periodic windows and we argue that this behaviour is associated with a heteroclinic bifurcation. In §4 we explore the development of chaos on the oscillatory branch as R_S is increased. Finally, in §5, we assess the significance and limitations of our study and suggest directions for future research.

2. Survey of the problem

2.1. *The governing equations*

Two-dimensional thermosolutal convection in a layer of fluid, confined between infinite plane horizontal boundaries maintained at constant temperature and solute concentration, is described, in the Boussinesq approximation, by the non-dimensional equations (Huppert & Moore 1976)

$$\frac{1}{\sigma}[\partial_t \nabla^2 \Psi + J(\Psi, \nabla^2 \Psi)] = R_T \partial_x \Theta - R_S \partial_x \Sigma + \nabla^4 \Psi, \tag{1}$$

$$\partial_t \Theta + J(\Psi, \Theta) = \partial_x \Psi + \nabla^2 \Theta, \tag{2}$$

$$\partial_t \Sigma + J(\Psi, \Sigma) = \partial_x \Psi + \tau \nabla^2 \Sigma. \tag{3}$$

Here $\Psi(x, z, t)$ is the non-dimensionalized stream function, such that the velocity $(u, 0, w) = (-\partial_z \Psi, 0, \partial_x \Psi)$, and $\Theta(x, z, t)$, $\Sigma(x, z, t)$ denote respectively the departures of the temperature T and solute concentration S from their linear profiles present in the non-convecting state:

$$T - T_0 = \Delta T(1 - z + \Theta), \quad S - S_0 = \Delta S(1 - z + \Sigma). \tag{4}$$

Distances are measured in terms of the depth h of the convecting layer, and time in terms of the thermal conduction time h^2/κ_T. The four dimensionless parameters appearing in (1)–(3) are, respectively, the thermal and solutal Rayleigh numbers

$$R_T = \frac{g\alpha \Delta T h^3}{\kappa_T \nu}, \quad R_S = \frac{g\beta \Delta S h^3}{\kappa_T \nu}. \tag{5}$$

and the two Prandtl numbers

$$\sigma = \frac{\nu}{\kappa_T}, \quad \tau = \frac{\kappa_S}{\kappa_T}, \tag{6}$$

where ν is the viscous diffusivity. In (5), $\alpha = -(1/\rho)(\partial\rho/\partial T)|_S$ and $\beta = (1/\rho)(\partial\rho/\partial S)|_T$, the acceleration due to gravity is $(0, 0, -g)$, and ΔT, ΔS are, respectively, the temperature and solute differences imposed across the layer, with the lower boundary hotter and 'saltier' than the upper boundary. Finally, the symbol $J(f, g)$ denotes the Jacobian $\partial(f, g)/\partial(x, z)$. The density contrast across the layer is measured by the stability parameter (or density anomaly ratio) $\Lambda = \beta \Delta S/\alpha \Delta T \equiv R_S/R_T$. If the initial density increases with depth, then $\Lambda > 1$.

We consider convection cells of unit height and width 2λ, each occupied by two rolls of width λ, with opposite senses of motion. Then the system is periodic in x, with period 2λ, and we need only solve the equations in the region $\{0 \leqslant x \leqslant \lambda; 0 \leqslant z \leqslant 1\}$. For simplicity we assume reflection symmetry about the plane $x = 0$ (so that there is no flow or flux across the lateral boundaries) and impose stress-free boundary conditions at top and bottom. Then

$$\Psi = \partial_z^2 \Psi = \Theta = \Sigma = 0 \quad \text{on } z = 0, 1, \tag{7}$$

$$\Psi = \partial_x^2 \Psi = \partial_x \Theta = \partial_x \Sigma = 0 \quad \text{on } x = 0, \lambda. \tag{8}$$

Equations (1)–(3), (7) and (8) define the basic system to be studied. We note that this system also possesses a further symmetry, for it is invariant under the transformation

$$\begin{pmatrix} x \\ z \end{pmatrix} \to \begin{pmatrix} \lambda - x \\ 1 - z \end{pmatrix}, \quad \begin{pmatrix} \Psi \\ \Theta \\ \Sigma \end{pmatrix} \to \begin{pmatrix} \Psi \\ -\Theta \\ -\Sigma \end{pmatrix}. \tag{9}$$

The efficiency of double-diffusive convection is conveniently described by the thermal and solutal Nusselt numbers N_T and N_S defined by

$$N_T(z, t) - 1 = \frac{1}{\lambda} \int_0^\lambda dx \, (-\partial_z \Theta + w\Theta), \quad N_S(z, t) - 1 = \frac{1}{\lambda} \int_0^\lambda dx \, (-\partial_z \Sigma + w\Sigma). \tag{10}$$

These Nusselt numbers measure the rates at which heat and salinity are transported across the layer in the convective state relative to those in the (unstable) conductive state. Time averages of these Nusselt numbers will be denoted by $\bar{N}_T$ and $\bar{N}_S$, and both are independent of z if the convection is statistically steady. Of some importance in laboratory studies of thermosolutal convection is the variation of the destabilizing buoyancy flux carried through a layer with the stability parameter Λ. An average value of the buoyancy–flux ratio $\chi = \beta F_S / \alpha F_T$, where F_S and F_T are the dimensional solute and heat fluxes respectively, can be expressed in terms of N_S and N_T as

$$\bar{\chi} \equiv \tau \Lambda \frac{\bar{N}_S}{\bar{N}_T}. \tag{11}$$

For $\Lambda \gtrsim 2$, the buoyancy–flux ratio in various experiments is strikingly insensitive to Λ (cf. Turner 1973, chapter 8; Gough & Toomre 1982). For oscillatory solutions we find that $\bar{\chi}$ varies by 7 % while Λ increases by 20 %.

2.2. *Small-amplitude theory*

The system (1)–(3) with the boundary conditions (7) and (8) admits the pure conduction solution $\Psi = \Theta = \Sigma = 0$ for all values of the Rayleigh number R_T. In this section we summarize the linear stability properties of this trivial solution (e.g. Baines & Gill 1969; Huppert & Moore 1976), and discuss the small-amplitude nonlinear solutions present near the onset of instability.

The stability properties of the conduction solution are most conveniently described in terms of normalized Rayleigh numbers $r_T = R_T / R_0$, $r_S = R_S / R_0$, where $R_0 = \pi^4 (1 + \lambda^2)^3 / \lambda^4$ is the critical Rayleigh number for the onset of convection in the absence of a solute gradient. As r_T is increased, the conduction solution loses stability to growing oscillations at

$$r_T = r_T^{(0)} \equiv 1 + (1 + \sigma + \tau) \frac{\tau}{\sigma} + \left(\frac{\sigma + \tau}{\sigma + 1}\right) r_S, \tag{12}$$

provided that $\tau < 1$ and

$$r_S > r_S^{(c)} \equiv \frac{\tau^2}{\sigma}\left(\frac{1+\sigma}{1-\tau}\right) > 0. \tag{13}$$

Thus there is an oscillatory (or Hopf) bifurcation at $r_T = r_T^{(o)}$, corresponding to the onset of overstability, if (13) is satisfied. These conditions are in agreement with the physical argument presented in §1. The frequency of the neutrally stable oscillations at $r_T = r_T^{(o)}$ is given by

$$\Omega^2 = -\tau^2 + \left(\frac{1-\tau}{1+\sigma}\right)\sigma r_S > 0. \tag{14}$$

As r_T is increased beyond $r_T^{(o)}$ the frequency of the overstable oscillations in the linearized system decreases to zero at $r_T = r_T^{(1)}$ and for $r_T > r_T^{(1)}$ there are two real positive eigenvalues, one of which passes through zero when r_T reaches

$$r_T^{(e)} \equiv 1 + r_S/\tau. \tag{15}$$

The stationary bifurcation at $r_T = r_T^{(e)}$ corresponds to the exchange of stabilities, and $r_T^{(e)} > r_T^{(o)}$ if (13) is satisfied. A branch of oscillatory solutions bifurcates from $r_T^{(o)}$; the bifurcation may be either subcritical or supercritical (Huppert & Moore 1976; Da Costa *et al.* 1981). Similarly, a branch of steady solutions bifurcates from $r_T^{(e)}$. This bifurcation is always subcritical if convection sets in as overstable oscillations $(r_T^{(o)} < r_T^{(e)})$. Thus there are small-amplitude steady solutions for $r_T \lesssim r_T^{(e)}$. These solutions are unstable with one $O(1)$ unstable eigenvalue.

Nonlinear solutions to (1)–(3), (8) and (9) can be found when $r_S = r_S^{(c)} + \epsilon^2$, $\epsilon \ll 1$ (Knobloch & Proctor 1981). Then the amplitude of the oscillations is $O(\epsilon)$, while their frequency is also $O(\epsilon)$. In this case the whole branch of oscillatory solutions is accessible to perturbation theory. The calculation shows that the oscillatory branch terminates on the branch of unstable steady solutions that bifurcates subcritically from $r_T^{(e)}$, with the formation of an infinite period heteroclinic orbit at $r_T^{(c)}$ joining two saddlepoints corresponding, respectively, to unstable clockwise and unstable anticlockwise rolls. Structural stability considerations (Arnol'd 1977, 1983; Gucken-heimer & Knobloch 1983) show that the heteroclinic orbit persists for finite values of ϵ. The existence of this heteroclinic orbit will be important in what follows. In figure 1 (*a*) we show the bifurcation diagram for this case and in figure 1 (*b*) the heteroclinic orbit at $r_T^{(c)}$.

2.3. *Previous numerical studies*

For larger amplitudes equations (1)–(3), (8) and (9) have to be solved numerically. This was first done by Veronis (1968) using a truncated Fourier representation, and subsequently by Huppert & Moore (1976) employing a second-order finite-difference scheme (Moore, Peckover & Weiss 1974). Huppert & Moore were able to reach larger supercritical Rayleigh numbers and hence larger amplitudes. They also found the first example of a transition from periodic to aperiodic solutions for a system of partial differential equations. Since their study serves as the starting point for the present paper, we summarize below those of their results that are particularly relevant.

Huppert & Moore computed finite amplitude time-independent solutions corre-sponding to stable steady overturning convection as a function of the Rayleigh num-ber R_T for several values of the solutal Rayleigh number R_S, and determined the minimum Rayleigh number $R_T^{\min}$, for which such solutions existed. They were also able to follow the branch of oscillatory solutions from $R_T^{(o)}$ to larger amplitudes, and to investigate its development as a function of R_S. Such results are conveniently
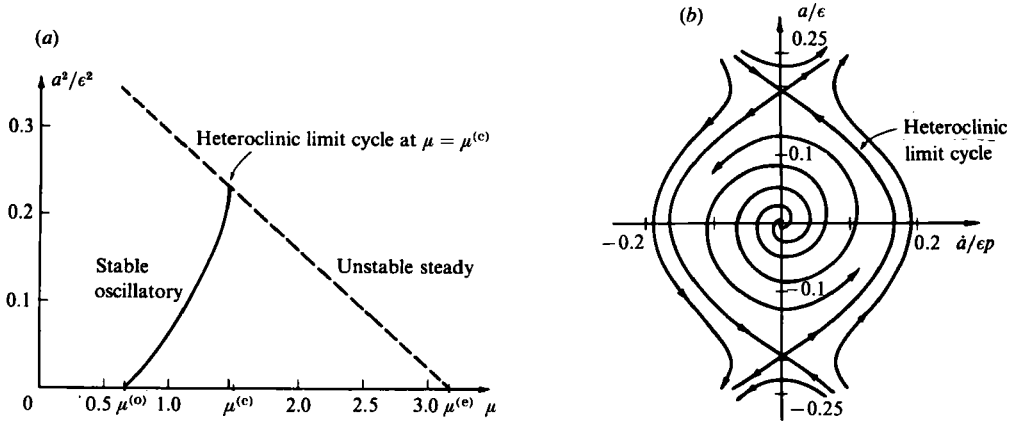
FIGURE 1. (a) Analytical amplitude–Rayleigh number $(a$–$r_T)$ diagram for the partial differential equations with $\sigma = 1.0$, $\tau = 0.316$ and $r_S = r_S^{(c)} + \epsilon^2$, $\epsilon \ll 1$, showing that the branch of oscillatory solutions (solid line) terminates on the branch of unstable steady solutions (broken line) at $\mu = \mu^{(c)} \simeq 1.468$, where $\mu = (r_T - 1.925)/\epsilon^2$. (b) Phase portrait at $r_T = r_T^{(c)}$ showing a heteroclinic limit cycle joining two saddle points (after Knobloch & Proctor 1981).
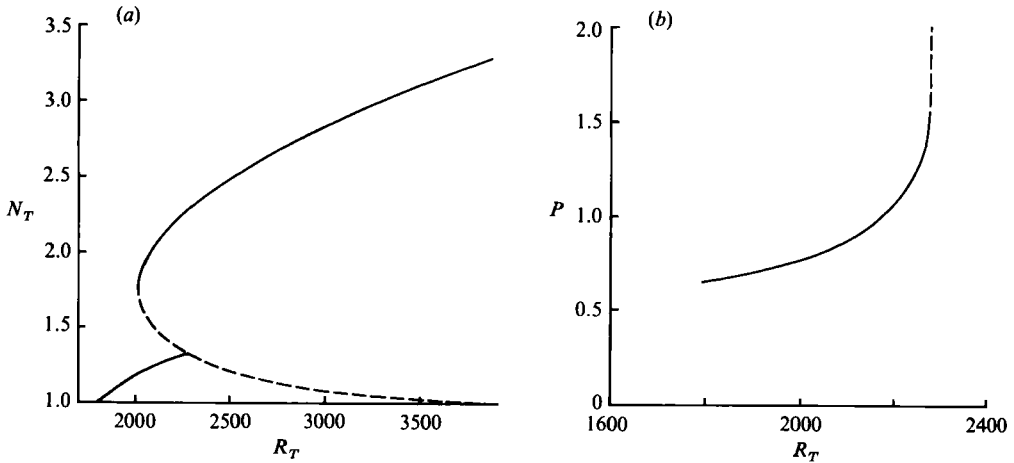

FIGURE 2. (a) Numerical Nusselt number–Rayleigh number $(N_T$–$R_T)$ diagram for the partial differential equations with $\lambda = 1.414$, $\sigma = 1.0$, $\tau = 0.316$ and $R_S = 10^3$ showing that the branch of oscillatory solutions still terminates on the branch of unstable steady solutions at $R_T^{(c)} \simeq 2280$. (b) The period P of the oscillations as R_T approaches $R_T^{(c)}$. The sharp rise in the period is characteristic of the approach to the heteroclinic limit cycle (after Huppert & Moore 1976).

represented in an amplitude–Rayleigh number diagram (cf. figure 1a), with the amplitude of motion measured by the thermal or solutal Nusselt numbers N_T,N_S evaluated, say, at the bottom of the layer $(z = 0)$. For $\lambda = 2^{\frac{1}{2}}$, $\sigma = 1$, $\tau = 10^{-\frac{1}{2}}$ and $R_S = 10^3$, Huppert & Moore found that the solutions along the oscillatory branch became more obviously nonlinear with increasing R_T, and disappeared beyond $R_T \approx 2275$ (see figure 2a). In figure 2(b) we show the period P of the oscillations along the oscillatory branch. As the end of the branch is approached the period increases rapidly. For $R_S = 10^{3.5}$, Huppert & Moore located a transition before the end of the oscillatory branch at which the period of the Nusselt numbers $N_T(t)$ and $N_S(t)$

doubled. No further transitions were found and the branch terminated at $R_T \approx 4450$. For $R_S = 10^4$, however, the first transition at $R_T \approx 9300$ was followed by a second transition at $R_T \approx 10000$ beyond which the oscillations were observed to be aperiodic. These oscillations disappeared at $R_T \approx 11100$. Calculations with $\lambda = 2^{\frac{1}{2}}$, $\sigma = 1$, $\tau = 10^{-1}$ and $R_S = 10^{3.5}$ showed similar behaviour, with the two transitions occurring at $R_T \approx 3350$ and $R_T \approx 3550$ before the branch ended at $R_T \approx 4150$. No other transitions were found in spite of some effort. Huppert (1976) concluded that aperiodicity in this system did not come about via a cascade of period-doubling bifurcations. In the following section we show that period doubling does occur, but that Huppert (1976, 1977) and Huppert & Moore (1976) were mistaken in identifying the period-doubling in the Nusselt numbers as the first period-doubling bifurcation. It is a bifurcation to asymmetrical oscillations. We shall argue that these bifurcations are intimately connected with the presence of the branch of unstable steady solutions (cf. figure 2a) and the existence of a heteroclinic orbit at the end of the oscillatory branch, as suggested by figure 2(b).

2.4. *A cascade of period-doubling bifurcations*

The eigenfunctions of the linear problem discussed in §2.2 have the form $\Psi = \Psi_{11}(t) \sin(\pi x/\lambda) \sin \pi z$, and it can be shown that nonlinear interactions generate solutions with the form

$$\Psi = \sum_m \sum_n \Psi_{mn}(t) \sin\left(\frac{m\pi x}{\lambda}\right) \sin n\pi z \quad (m+n \text{ even}) \tag{16}$$

(Veronis 1968). These solutions have the same symmetry (9) as the system being studied, corresponding to *spatial* symmetry about the centre of the convection roll, such that

$$\Psi(x,z) = \Psi(\lambda-x, 1-z), \quad \Theta(x,z) = -\Theta(\lambda-x, 1-z), \quad \Sigma(x,z) = -\Sigma(\lambda-x, 1-z). \tag{17}$$

Such solutions may still be unstable to perturbations that violate this symmetry; indeed, it is known from numerical studies of two-dimensional Rayleigh–Bénard convection (Curry *et al.* 1984) and magnetoconvection (Proctor & Weiss 1982; Arter 1983) that symmetry-breaking bifurcations can occur. We shall nevertheless follow Veronis (1968) and Huppert & Moore (1976) in imposing the spatial symmetry of (9) and (17) upon our solutions, in order to reduce computing time. This is a stringent requirement, which suppresses any symmetry-breaking bifurcations, but it allows detailed comparison of our results with earlier work and, more important, permits us to relate numerical experiments with the partial differential equations to the behaviour of the fifth-order model introduced in §2.5 below.

Periodic oscillations may also possess a *temporal* symmetry, relating solutions separated by half the period. For an extended layer this symmetry implies that increasing time by $\frac{1}{2}P$ is equivalent to horizontal translation by a distance λ, so that clockwise and anticlockwise motions are always similar. For a single roll, increasing time by $\frac{1}{2}P$ is equivalent to reflection about the plane $x = \frac{1}{2}\lambda$ and the symmetry is given by

$$\begin{pmatrix} x \\ z \\ t \end{pmatrix} \rightarrow \begin{pmatrix} \lambda-x \\ z \\ t+\frac{1}{2}P \end{pmatrix}, \quad \begin{pmatrix} \Psi \\ \Theta \\ \Sigma \end{pmatrix} \rightarrow \begin{pmatrix} -\Psi \\ \Theta \\ \Sigma \end{pmatrix}. \tag{18}$$
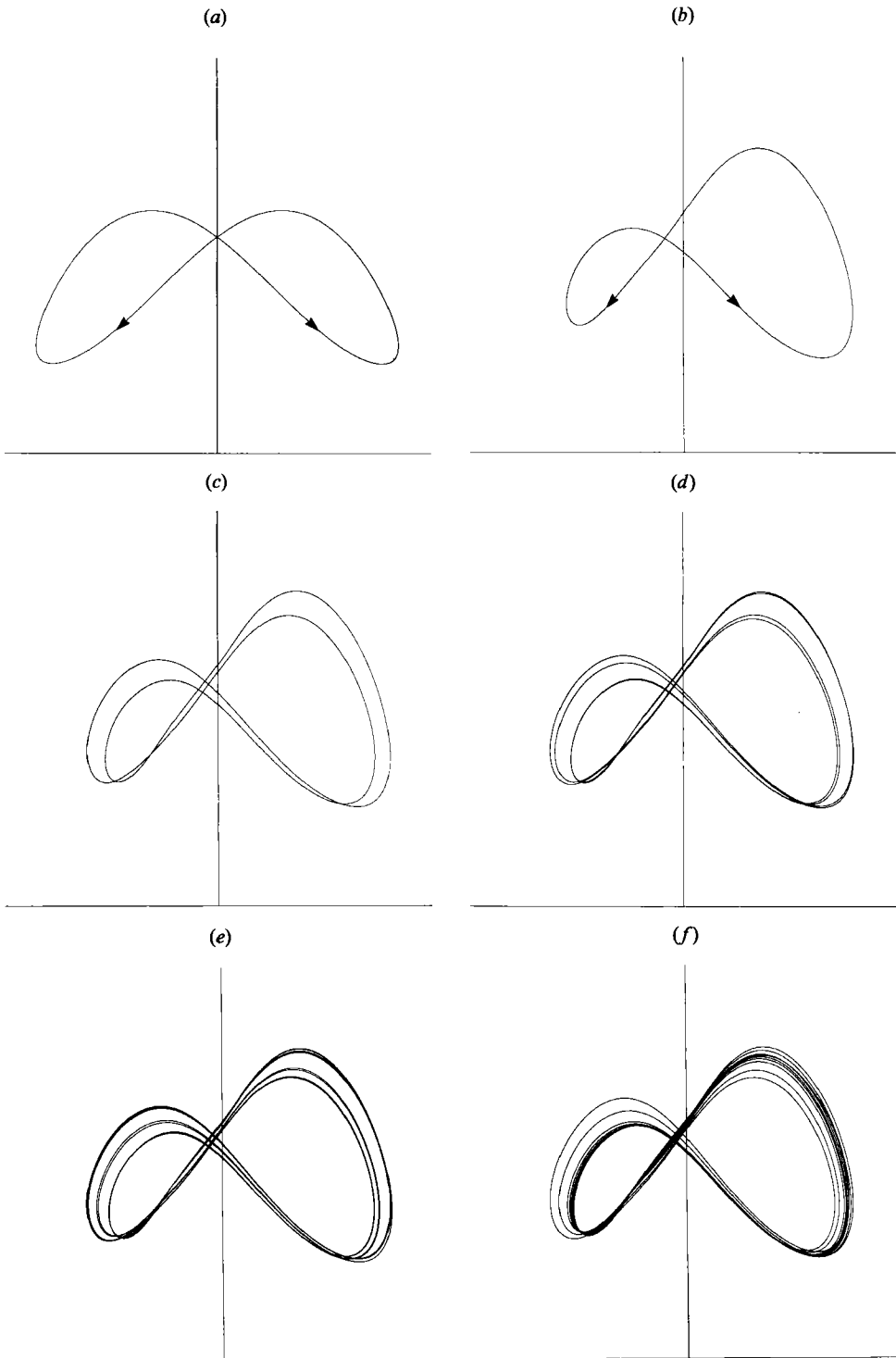
FIGURE 3. Solutions of the partial differential equations: plots of solutal Nusselt number (N_S) against horizontally averaged velocity on the lower boundary ($\langle u \rangle$) for $\lambda = 1.414$, $\sigma = 1.0$, $\tau = 0.316$, $R_S = 10^4$. Shown are (a) $R_T = 8600$ (symmetrical limit cycle); (b) $R_T = 10000$ (asymmetrical); (c) $R_T = 10100$ (period 2); (d) $R_T = 10120$ (period 4); (e) $R_T = 10150$ (chaotic); and (f) $R_T = 10200$ (chaotic).

Combining this temporal symmetry with the spatial symmetry (9), we find that

$$\begin{aligned}
\Psi(x,z,t) &= -\Psi(x,1-z,t+\tfrac{1}{2}P), \\
\Theta(x,z,t) &= -\Theta(x,1-z,t+\tfrac{1}{2}P), \\
\Sigma(x,z,t) &= -\Sigma(x,1-z,t+\tfrac{1}{2}P).
\end{aligned} \tag{19}$$

This symmetry obviously holds for the marginally stable oscillation at $r_T = r_T^{(o)}$, with $\Psi_{11} \propto \cos(2\pi t/P)$, and persists throughout the small-amplitude regime discussed in §2.2. A consequence of the symmetry is that quadratic measures of the convective efficiency, such as the mean kinetic energy E, or the Nusselt numbers N_T and N_S, do not depend on the sense of motion in the roll and therefore have a period of $\tfrac{1}{2}P$, instead of P.

In order to understand the nature of the first transition discovered by Huppert & Moore (1976) we have used their numerical code to obtain detailed solutions of (1)–(3), (8) and (9). In figures 3(a,b) we show the solution for $\lambda = 2^{\frac{1}{2}}$, $\sigma = 1$, $\tau = 10^{-\frac{1}{2}} \approx 0.316$, $R_S = 10^4$ before $(R_T = 8600)$ and after $(R_T = 10000)$ the transition, projected onto the $(\langle u \rangle, N_S)$-plane, where $\langle u \rangle$ is the horizontally averaged horizontal velocity along the lower boundary,

$$\langle u \rangle = \frac{1}{\lambda} \int_0^\lambda u(x,0,t)\,\mathrm{d}x, \tag{20}$$

and N_S is evaluated at $z = 0$. These projections show clearly that there is a transition from a symmetrical limit cycle (where $\langle u \rangle$ has period P but N_S has period $\tfrac{1}{2}P$) to an asymmetrical limit cycle in which clockwise and anticlockwise motion no longer have the same amplitude (and both $\langle u \rangle$ and N_S have period P). Temporal symmetry is broken by a (supercritical) pitchfork bifurcation, in which the symmetrical solution loses stability and a pair of stable asymmetrical solutions are created. These two solutions transform into one another under the symmetry (18); which one is realized depends on the initial conditions. This breaking of symmetry is manifested as an apparent period-doubling in N_T, N_S, and E.

Equations (1)–(3), (8) and (9) do, however, exhibit true period-doubling bifurcations. Indeed, a bifurcation to asymmetry is a necessary prerequisite for period doubling (see §3.4 below). In figure 3(c,d) we show a period-2 and a period-4 solution in the $(\langle u \rangle, N_S)$-plane. These solutions are present for $R_T = 10100$ and $R_T = 10120$. Observe that the period-2 solution describes the asymmetrical cycle twice before closing. As R_T is further increased more period-doubling bifurcations can be found. The bifurcation points appear to accumulate rapidly; beyond the accumulation point aperiodic solutions are found. We show examples of two such solutions in figures 3(e,f) for $R_T = 10150$ and $R_T = 10200$. From these figures the relationship of the aperiodic solutions to the periodic solutions can easily be seen. The structure of the aperiodic regime is, however, very complex; we return to it in much greater detail in §3.

2.5. *Fifth-order model system*

Equations (1)–(3), (8) and (9) can be modelled by a system of five ordinary differential equations originally suggested by Veronis (1965):

$$\dot{a} = \sigma[-a + r_T b - r_S d], \tag{21}$$

$$\dot{b} = -b + a(1-c), \tag{22}$$

$$\dot{c} = \varpi(-c + ab), \tag{23}$$

$$\dot{d} = -\tau d + a(1-e), \tag{24}$$

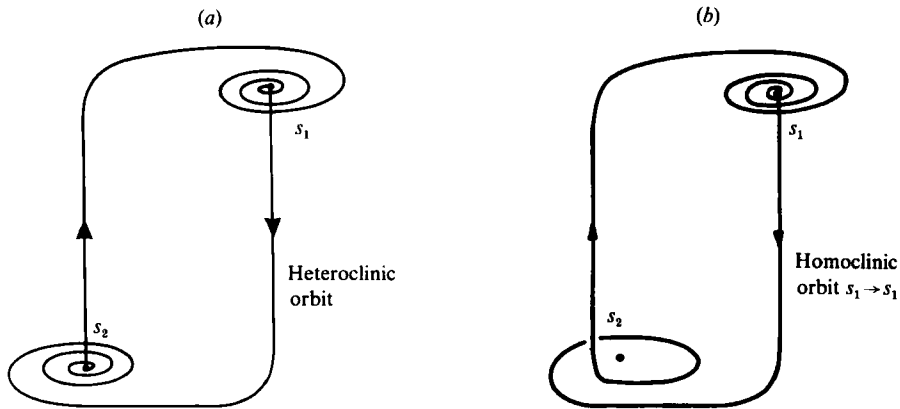$$\dot{e} = \varpi(-\tau e + ad), \tag{25}$$

FIGURE 4. The fifth-order model: (a) Sketch of a heteroclinic limit cycle connecting saddle-foci; (b) Sketch of a possible homoclinic limit cycle.

where $\varpi = 4\pi^2/p$, $p = \pi^2(1+1/\lambda^2)$, and differentiation is with respect to a scaled time $t^* = pt$. The variables a, b and d represent the amplitudes of the linear eigenmodes of Ψ, Θ and Σ respectively; c and e provide a primitive representation of the thermal and solutal boundary layers at the top and bottom of the layer as described by second-order perturbation theory (cf. Da Costa et al. 1981). The symmetry of the original problem with respect to horizontal translations by a distance λ corresponds to the symmetry

$$a \to -a, \quad b \to -b, \quad c \to c, \quad d \to -d, \quad e \to e, \qquad (26)$$

of the model. By construction the model equations have the same linear and small-amplitude properties as (1)–(3). At larger amplitudes the model equations favour subcritical convection because they neglect the deceleration of the velocity, described by the amplitude a, in the solutal boundary layers at the top and bottom of the cell. However, (21)–(25) have the virtue that steady solutions can be found analytically and their stability properties easily ascertained. The model shows that the subcritical branch of unstable steady solutions that bifurcates off the trivial conduction solution $a = b = c = d = e = 0$ at $r_T^{(e)}$ turns around at $r_T = r_T^{\min}$ where it acquires stability (Da Costa et al. 1981). Thus the stable subcritical finite-amplitude overturning solutions present for $r_T > r_T^{\min}$ are connected to $r_T^{(e)}$ by a branch of unstable steady solutions. We conjecture that this is also true for the partial differential equations, as indicated in figure 2(a).

The model equations can easily be integrated numerically, and the development of the branch of oscillatory solutions as a function of the parameters can be mapped out in some detail. For values of r_S close to $r_S^{(e)}$ the results obtained by Knobloch & Proctor (1981) apply. The branch of oscillatory solutions then terminates at $r_T^{(c)}$ on the branch of unstable steady solutions in a heteroclinic orbit (cf. §2.2). Da Costa et al. (1981) showed numerically that the oscillatory branch continues to terminate on the unstable steady branch as r_S is increased. The nature of the heteroclinic orbit at $r_T^{(c)}(r_S)$ depends, however, on the eigenvalues along the steady branch. Close to $r_T^{(e)}$ there are one real positive (unstable) $O(1)$ eigenvalue s_1 and four real negative (stable) eigenvalues $s_2, \ldots, s_5$, one of which (s_2) is small since it vanishes at $r_T^{(e)}$; thus $s_1 > 0 > s_2 > s_3 > s_4 > s_5$. For r_S close to $r_S^{(c)}$ the unstable eigenvalue decreases along
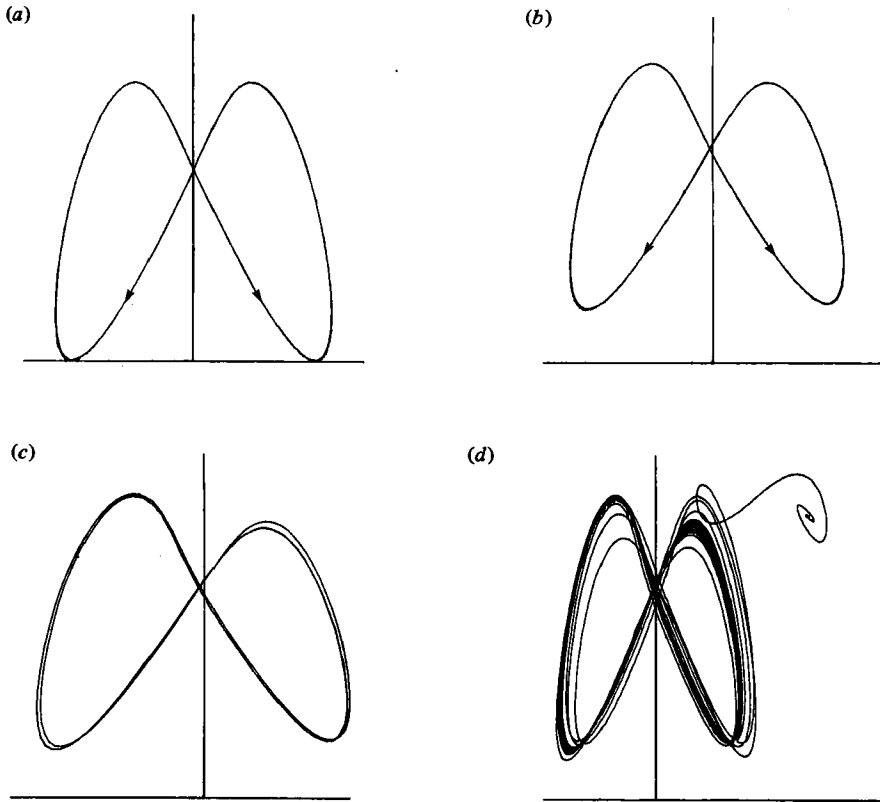
(a)

(b)

(c)

(d)

FIGURE 5. Solutions of the fifth-order model projected onto the (a, e)-plane for $\varpi = 8/3$, $\sigma = 1$, $\tau = 0.316$, $r_S = 15.0$ [$R_S = 9863$]. Shown are (a) $r_T = 13.4$ [$R_T = 8810$], symmetrical limit cycle; (b) $r_T = 13.5$ [$R_T = 8876$], asymmetrical limit cycle; (c) $r_T = 13.56$ [$R_T = 8916$], period 2 and (d) $r_T = 13.564$ [$R_T = 8918$], chaotic transient at the end of the oscillatory branch. These solutions should be compared with the analogous $\langle u \rangle$, N_S projections for the partial differential equations shown in figure 3.

the steady branch and passes through zero at $r_T^{\min}$. Beyond the turning point at $r_T^{\min}$ the steady branch is stable. The fixed points corresponding to clockwise and anticlockwise overturning convection thus have a one-dimensional unstable mani-fold, and a four-dimensional stable manifold. The heteroclinic orbit is tangent to the plane spanned by the unstable eigenvector and the eigenvector of the small stable eigenvalue (cf. figure 1 b). For larger values of r_S the small negative eigenvalue s_2 decreases along the steady branch until at r_T^* $s_2 = s_3$ ($> s_4$), and thereafter (i.e. for $r_T^* > r_T > r_T^{\min}$) these two eigenvalues lie in the complex plane. With the appearance of a pair of complex-conjugate eigenvalues the fixed points change from saddles into saddle-foci. A heteroclinic orbit joining the two saddle-foci spirals into one fixed point along a two-dimensional surface and emerges from the fixed point along the one-dimensional unstable manifold which takes it to the other saddle-focus where it again spirals into the fixed point. We show a sketch of such an orbit in figure 4 (a).

For comparison with the results described in §§ 2.3, 2.4, we take $\lambda = 2^{\frac{1}{2}}$ ($\varpi = \frac{8}{3}$), $\sigma = 1$, and $\tau = 10^{-\frac{1}{2}}$, and consider the effect of increasing r_S. At $r_S^{(c)} = 0.2929$, when the oscillations first occur, a pair of complex eigenvalues appears on the branch of

unstable steady solutions a short though finite distance from $r_T^{(e)} = r_T^{(o)} = 1.925$. When $r_S = 1$ there is a pair of complex eigenvalues on the unstable steady branch for $r_T^{\min} \simeq 2.283 \leqslant r_T \leqslant r_T^* \simeq 3.555$. The branch of oscillatory solutions terminates in a heteroclinic orbit at $r_T^{(c)} \simeq 2.833\,154\,2$, well within this region. It can be confirmed that the trajectory describes tight loops around the saddle-foci (cf. figure 16 of Knobloch & Weiss 1983) which are qualitatively similar to those in figure 4(a).

If we solve (21)–(25) for $r_S = 15$ ($R_S = 9863$) we can follow the oscillatory branch from $r_T^{(o)}$ for increasing values of r_T. Initially, the oscillations have a temporal symmetry, corresponding to (19), such that

$$a(t) = -a(t+\tfrac{1}{2}P), \quad b(t) = -b(t+\tfrac{1}{2}P), \quad d(t) = -d(t+\tfrac{1}{2}P),$$

$$c(t) = c(t+\tfrac{1}{2}P), \quad e(t) = e(t+\tfrac{1}{2}P). \tag{27}$$

We find at $r_T \approx 13.47$ a bifurcation to asymmetry, followed at $r_T \approx 13.55$ by the first period-doubling bifurcation (cf. Da Costa *et al.* 1981). In figure 5(a, b, c) we show examples of orbits that are symmetrical, asymmetrical and of period 2, projected on the (a, e)-plane. This plane is the analogue in the model problem of the $(\langle u \rangle, N_S)$-plane used for the full partial differential equations in §2.4. Figure 5 should be compared with figure 3. We see that the solutions of the model system are in qualitative agreement with those of equations (1)–(3), although the model solutions have less structure. Two more period-doubling bifurcations are easily located and occur at $r_T \approx 13.562$, and $r_T \approx 13.5631$; at $r_T \approx 13.5635$ the solution is aperiodic, and the oscillatory solutions disappear at $r_T \approx 13.564$. Figure 5(d) shows a trajectory for $r_T = 13.564$ which initially appears chaotic, but eventually spirals into the stable fixed point on the upper portion of the steady branch. Thus both the partial differential equations (1)–(3) and the fifth-order model (21)–(25) approach chaos by a period-doubling cascade. There are, however, significant differences between the two systems; we shall describe these in the following section.

3. Successive transitions in oscillatory behaviour at $\tau = 0.316$, $R_S = 10^4$

3.1. *Numerical procedure*

In this section we describe in detail our investigation of the solutions to the partial differential equations (1)–(3), (7) and (8) for the parameter values $\sigma = 1$, $\tau = 10^{-\frac{1}{2}} \approx 0.316$, $R_S = 10^4$. The survey carried out by Huppert & Moore (1976) suggested that this choice of parameters (plus another to be considered in §4) is especially promising for further study of transitions in time-dependent behaviour. The aspect ratio λ was chosen to be either $\lambda = 2^{\frac{1}{2}}$, the value that minimizes the Rayleigh number for onset of convection, or $\lambda = 1.5$, for convenience in defining the mesh. The qualitative aspects of the results are unchanged by increasing λ from 1.414 to 1.5, although individual bifurcations are displaced by up to 1.5%.

Two different numerical codes have been used for these investigations. Both codes use the finite-difference formulation of equations (1)–(3) presented by Moore *et al.* (1974) in which Ψ, $\nabla^2 \Psi$, Θ and Σ are specified on grids staggered in space and time. The difference scheme has second-order accuracy and is centred in both space and time; in stepping forward in time, the nonlinear terms are treated explicitly and the diffusive terms are represented by a Dufort–Frankel scheme. The associated Poisson equation linking stream function and vorticity is solved by Fourier decomposition and tridiagonal elimination. The code used to construct solutions for aspect ratio
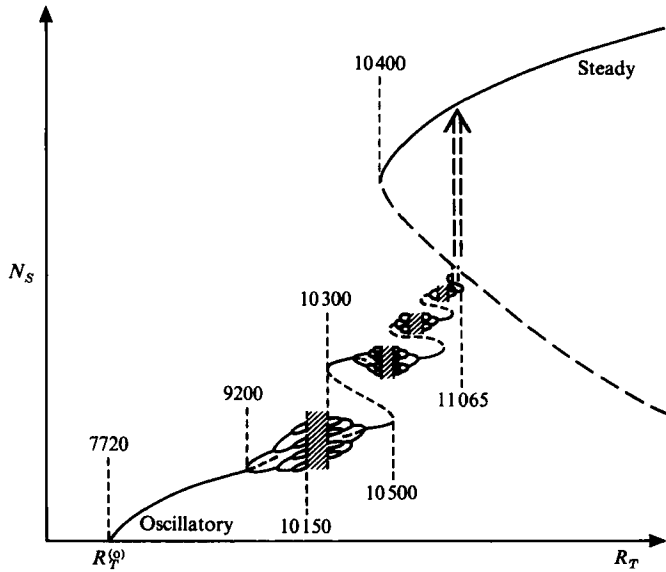
FIGURE 6. Steady and oscillatory solutions of the partial differential equations: schematic bifurcation diagram of the solutal Nusselt number N_S as a function of R_T. Note the bubbles of period-doubling bifurcations on the first and second oscillatory branches, the hysteresis loop connecting the two branches and subsequent (conjectured) branches. Conjectured unstable solutions are indicated by broken lines.

$\lambda = 2^{\frac{1}{2}}$ is the same as that used by Huppert & Moore. The other code has been structured to take particular advantage of vector computers like the Cray-1; it employs improved fast Fourier transform (FFT) algorithms (Moore 1985) and tridiagonal inversion techniques (Moore & Wallcraft 1986). The vector structure of this numerical code also significantly enhances the computational performance on computers like the DEC VAX.

Imposition of the spatial symmetry (17) means that we have to compute the variables explicitly over only half of the spatial computational domain. We typically employed 16 mesh intervals in the vertical and 12 in the horizontal direction, corresponding to 24 intervals over the range $0 \leqslant x \leqslant \lambda$. Such a mesh in effect yields a total of 594 independent variables, which may be contrasted with the five modes used in §2.5. Boundary-layer structures are adequately resolved by our computational grids. The grid resolution was doubled in both dimensions for certain runs, with a corresponding reduction in the time step, to test the accuracy of the finite-difference representation. In all cases described here, the bifurcation pattern appeared to be unaltered, though individual transitions were displaced by up to 1%. The value of $\tau = 0.316$ used here was chosen for computational convenience, following Veronis (1968) and Huppert & Moore; the solutal boundary layers at top and bottom are then broader and more easily resolved than they would be for thermohaline convection with $\tau = 0.01$ (e.g. Gough & Toomre 1982).

In characterizing the different kinds of solutions, we shall use kinetic-energy phase plots and associated power spectra. We define the kinetic energy E by

$$E(t) = \frac{1}{2} \int_0^1 \mathrm{d}z \int_0^\lambda \mathrm{d}x \, [(\partial_x \, \Psi)^2 + (\partial_z \, \Psi)^2] = -\frac{1}{2} \int_0^1 \mathrm{d}z \int_0^\lambda \mathrm{d}x \, \Psi \nabla^2 \Psi, \qquad (28)$$

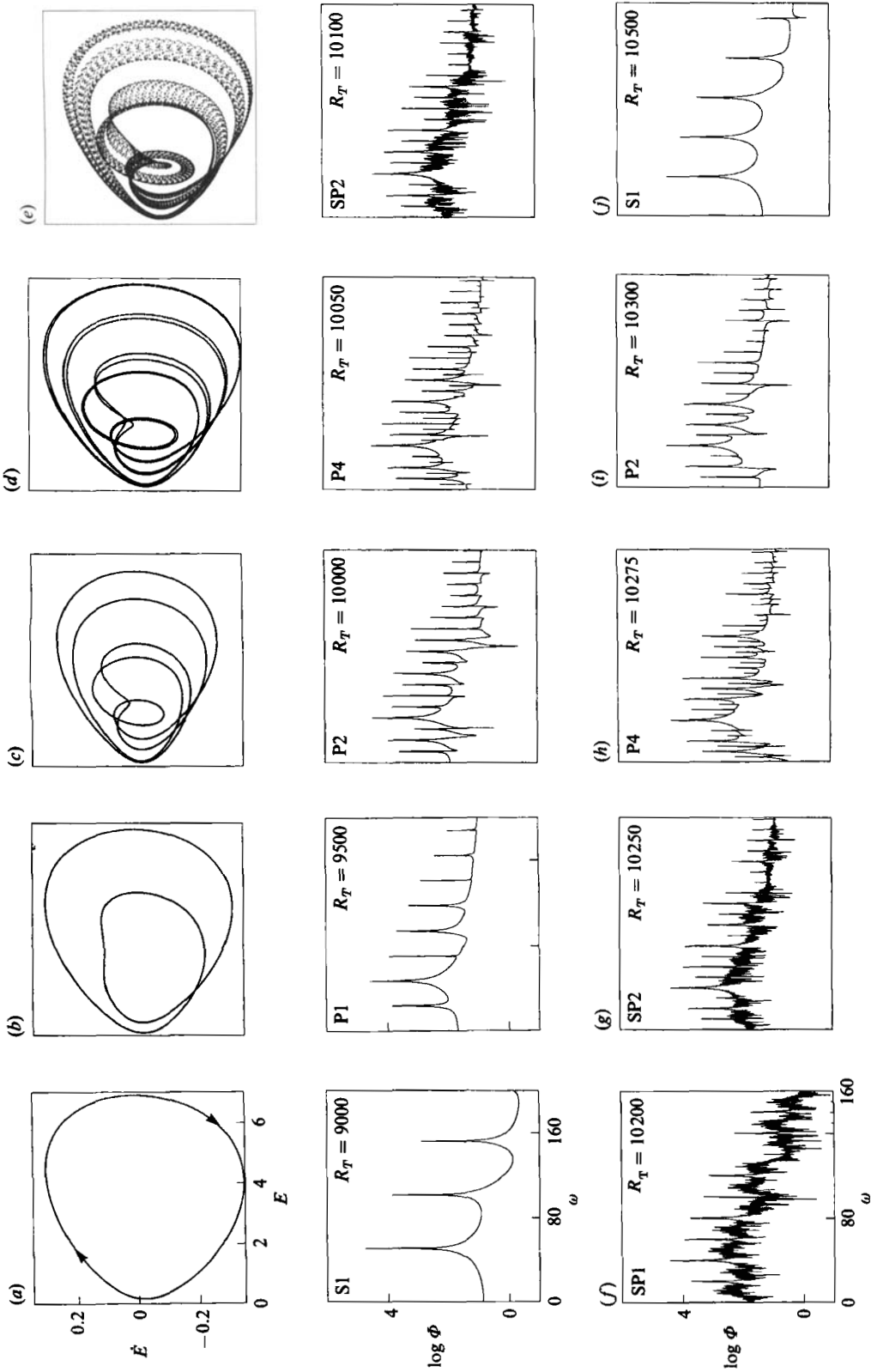E. Knobloch, D. R. Moore, J. Toomre and N. O. Weiss

FIGURE 7. Solutions of the partial differential equations: the first oscillatory branch for $\lambda = 1.5$, $\sigma = 1.0$, $\tau = 0.316$ and $R_S = 10^4$. Kinetic-energy phase plane plots ($\dot{E}$ vs. E with trajectories proceeding clockwise) and kinetic-energy power spectra Φ as a function of frequency ω for a succession of R_T values, showing period-doubling into chaos, semiperiodic solutions, and period-doubling out of chaos. Only the power spectra are shown for the last five R_T values. Each panel is labelled by the R_T value and the solution classification summarized in table 2.

and plot trajectories in the $(E, \dot{E})$ phase plane, where the overdot denotes a time derivative. The power spectrum is defined by

$$\Phi(\omega) = \left| \frac{1}{2T} \int_{-T}^{T} e^{i\omega t}\, E(t)\, \mathrm{d}t \right|^2, \tag{29}$$

and is evaluated for a sufficiently large T once the initial transient has decayed. The computation of the spectrum was accomplished by fast Fourier transforms. The details of the spectrum, though not the positions of the lines, depend somewhat on the commensurability of the length of the time series $2T$ with the period, $P = 2\pi/\omega_1$, of the periodic oscillations. If the time series is not an integral number of periods, the spectral lines are broadened. This artifact is easily distinguishable from real chaotic spectra and occurs at lower power levels. Since the computer runs were made for a predetermined number of time steps (typically $2^{15} = 32\,768$ steps after the initial transients had died away) and the period was *a priori* unknown it was not possible to obtain runs over an exact integral multiple of the period.

3.2. *The first oscillatory branch: bubble structure*

Figure 6 provides a schematic summary of the results to be described in this section. The amplitudes shown for oscillatory solutions are chosen so as to distinguish between products of pitchfork bifurcations. For $\lambda = 1.5$, the branch of oscillatory solutions bifurcates (supercritically) from the conduction solution when R_T reaches $R_T^{(o)} = 7720$. The amplitude of the oscillations increases with increasing R_T and the oscillations undergo a bifurcation from symmetry to asymmetry followed by a cascade of period-doubling bifurcations leading to semiperiodic chaotic solutions. These bifurcations are reversed as R_T increases further forming a complete bubble as described in §1. For larger values, solutions lie on a second oscillatory branch. We conjecture that the two branches are connected by a branch of unstable oscillations in a pair of saddle node (more precisely loop–loop) bifurcations as indicated. The solutions on the second oscillatory branch are different in form, and show a greater variety of behaviour. In particular the chaotic regime was interrupted by a number of periodic windows. Also sketched in figure 6 is the conjectured position of the branch of unstable steady solutions that bifurcates from $R_T^{(e)} = 32\,280$, together with the stable steady solutions present at large amplitudes for $R_T > R_T^{\min} \approx 10\,400$. We present first the results for the first oscillatory branch, followed by those for the second branch.

The small-amplitude oscillations present near the Hopf bifurcation at $R_T^{(o)}$ are symmetrical. An example of such a symmetrical solution of period 1, denoted as S1, is shown for $R_T = 9000$ in figure 7 (*a*). The motion in the upper $(E, \dot{E})$-phase-plane plot in figure 7 (*a*) is clockwise; the orbit describes two cycles during a full period and the second cycle repeats the first cycle exactly. For a symmetrical solution it is necessary that the fluid motions in the convection cell should have equal amplitudes during the rising and falling portions of the oscillation. The kinetic-energy power spectrum is shown in the lower panel of figure 7 (*a*). The basic period of this S1 solution is $P = 4\pi/\omega_0$ and the spectrum has power both at the fundamental frequency ω_0 and at its harmonics. These overtones control the shape of the orbit in the $(E, \dot{E})$-plane. As R_T is increased the oscillations undergo a bifurcation to asymmetry at $R_T \approx 9200$. In the energy phase plot shown for $R_T = 9500$ in figure 7 (*b*), the bifurcation to asymmetry is revealed by a difference in the trajectory during the two halves of the cycle. The two halves of the cycle separate only gradually as R_T is advanced beyond

the bifurcation point, implying that this bifurcation (like the subsequent period-doubling bifurcations) is supercritical. The kinetic-energy power spectrum in figure 7(b) now contains the two frequencies $\omega_1 \equiv \frac{1}{2}\omega_0$ and ω_0, along with their harmonics and sums and differences. We denote such a solution by P1 for asymmetrical period-1 solution. The first appearance of asymmetry beyond $R_T \approx 9200$ shows up as a very small peak in power at ω_1, with this peak becoming more prominent as the asymmetry is emphasized by increasing R_T.

The subsequent period-doubling bifurcations with increasing R_T also appear as gradual splittings of the trajectories in the $(E, \dot{E})$-plane and associated subharmonic peaks in the power spectrum. We give examples of a period-2 (P2) solution at $R_T = 10000$ in figure 7(c) and a P4 solution at $R_T = 10050$ in figure 7(d). These period-doubling bifurcations manifest themselves by the appearance of new peaks in the kinetic-energy spectra corresponding to $\frac{1}{2}\omega_1$ and $\frac{1}{4}\omega_1$ and sums and differences with the other frequencies already present. Comparison of orbits for these P2 and P4 solutions with that of the P1 solution in figure 7(b) reveals the presence of a distinctive additional loop in the period-doubled orbits as the trajectories traverse the neighbourhood of one of the two saddle points.

We have located one more period-doubled solution (P8) at $R_T = 10070$, and our surveys of the solutions are consistent with a Feigenbaum sequence of period-doubling bifurcations that accumulates at some finite value of R_T at an asymptotically geometric rate. The precise determination of the bifurcation points would require many more solutions than we have been able to obtain, given constraints on computing resources. Beyond the accumulation point, estimated to be at $R_T \approx 10075$, we find aperiodic solutions. In the spectrum the peaks broaden dramatically and as R_T is increased the lower frequency peaks (and harmonics) get successively submerged in the noise. We illustrate this with solutions at $R_T = 10100$ (figure 7e) and $R_T = 10200$ (figure 7f). The first of these is a semiperiodic solution of period 2 (SP2). This term was introduced by Lorenz (1979) to describe a solution that oscillates predictably between two regions of phase space without ever repeating itself. In the power spectrum in figure 7(e) this is manifested by peaks at $\frac{1}{2}\omega_1$, ω_1, and ω_0 and harmonics, and the spectrum contains a characteristic broadband component. The $(E, \dot{E})$-plot resembles a twisted ribbon with a prominent kink as the solution passes the saddle point. What is probably being seen in projection is an attractor that forms a low-dimensional flattened 'tube' in the phase space. (Note that points are plotted after each time step; for periodic solutions this procedure eventually generates a closed curve but aperiodic trajectories retain a fuzzy appearance.) As R_T is increased to 10200 the peaks in power corresponding to $\frac{1}{2}\omega_1$ (and harmonics) disappear; the solution is now SP1 (an asymmetrical semiperiodic solution of period 1). For brevity, in this figure 7(f) and in the subsequent panels only the power spectra are shown. As R_T is further increased the preceding bifurcations occur in reverse, until a symmetric S1 solution is again established. Thus in the SP2 solution at $R_T = 10250$, shown in figure 7(g), the $\frac{1}{2}\omega_1$ peak has reappeared in the power spectrum, while the subsequent solutions shown are a distinctive period 4 (P4) at $R_T = 10275$ in figure 7(h), a P2 at $R_T = 10300$ in figure 7(i), and finally a symmetrical S1 solution with only ω_0 and its harmonics present in the spectrum at $R_T = 10500$ in figure 7(j). The precise value of the frequency ω_0 changes slowly with R_T; note that the ω_0 peak consistently possesses the greatest power (in the log-Φ scales plotted here) in all of these different solutions and can readily be identified.

Details of all these illustrated solutions (and those in subsequent figures) are given in table 1. In particular, table 1 lists the fundamental frequency ω_0, the time-averaged

R_T	Type	ω_0	$\bar{E}$	$\bar{N}_T$	$\bar{N}_S$	$\bar{\chi}$
		First oscillatory branch				
9000	S1	50.752	3.061	1.690	2.254	0.04687
9500	P1	46.985	2.617	1.665	2.298	0.04596
10000	P2	41.993	2.268	1.671	2.392	0.04525
10050	P4	41.406	2.247	1.674	2.409	0.04525
10100	SP2	40.930	2.221	1.676	2.423	0.04521
10200	SP1	40.087	2.167	1.674	2.437	0.04516
10250	SP2	39.719	2.136	1.672	2.443	0.04511
10275	P4	39.417	2.124	1.673	2.449	0.04508
10300	P2	39.232	2.110	1.673	2.458	0.04505
10500	S1	37.135	1.968	1.667	2.474	0.04470
		Second oscillatory branch				
10300	S1	32.693	2.352	1.823	2.700	0.04548
10470	P4	30.961	2.378	1.846	2.792	0.04567
10472	SP8	30.964	2.378	1.846	2.792	0.04567
10475	SP2	30.968	2.373	1.845	2.791	0.04566
10485	SP1	30.865	2.385	1.850	2.802	0.04569
10508	IS3	31.017	2.320	1.831	2.770	0.04551
10510	S3	31.256	2.274	1.817	2.737	0.04533
10515	P3	31.263	2.262	1.813	2.730	0.04530
10520	SS3	31.034	2.296	1.824	2.756	0.04542
10575	IP2	31.707	2.162	1.781	2.679	0.04498
10600	P2	31.626	2.127	1.768	2.659	0.04485
10625	C	—	2.189	1.795	2.717	0.04507
11000	C	—	2.217	1.834	2.856	0.04477

TABLE 1. Properties of illustrated numerical solutions of partial differential equations for aspect ratio $\lambda = 1.5$, with $R_S = 10^4$, $\tau = 0.316$ and $\sigma = 1$

kinetic energy $\bar{E}$, the time-averaged Nusselt numbers $\bar{N}_T$ and $\bar{N}_S$, and the associated buoyancy flux ratio $\bar{\chi}$. A summary classification by solution type of all runs made with $\lambda = 1.5$ is given in table 2.

In figure 8 we present a brief segment of the time series for the P4 solution found at $R_T = 10050$. In figure 8(a) we show the vertical velocity $w(x = 0, z = \frac{1}{2}, t)$ and for comparison in figure 8(b) the kinetic energy $E(t)$. Note the splitting in successive maxima or minima. The presence of many Fourier components is clearly evident and, although one can reasonably guess at the periodicities involved, the power spectrum in figure 7(d) is needed to remove any ambiguities. Finally in figures 8(c) and (d) we show $N_T(z = \frac{1}{2}, t)$ and $N_S(z = \frac{1}{2}, t)$.

The results obtained for the first oscillatory branch are summarized schematically in figure 6. The double passage through the bifurcation sequence has a bubble-like structure and we shall refer to such a double sequence, here from S1 to semiperiodicity and back to S1, as a bubble. Typically, we might expect to find brief intervals of R_T with periodic solutions, lying within the range of chaotic behaviour, but we have not located any such periodic windows in the centre of this bubble.

3.3. *The second oscillatory branch: periodic windows*

The first oscillatory branch ends at $R_T \approx 10500$, and for $R_T > 10500$ the solutions settle on the second oscillatory branch. This branch can be extended to smaller R_T

First oscillatory branch		Second oscillatory branch	
R_T	Solution type	R_T	Solution type
8000	S1		
9000	S1		
9100	S1		
9200	P1		Evolves to
9250	P1	10275	first branch
9500	P1	10300	S1
9750	P1	10400	P1
9900	P2	10450	P1
9950	P2	10465	P2
10000	P2	10470	P4
10050	P4	10471	P4
10065	P4	10472	SP8
10070	P8	10475	SP2
10075	C	10485	SP1
10100	SP2	10500	SP1
10200	SP1	10505	SP1
10250	SP2	10508	IS3
10275	P4	10510	S3
10300	P2	10515	P3
—		10516	P6
—		10517	SP3
10500	S1	10520	SS3
10505	Evolves to	10525	SP1
	second branch	10550	C
		10575	IP2
		10600	P2
		10625	C
		10650	C
		10675	IS3
		10690	SP3
		10700	P3
		10725	C
		10750	C
		10775	S3
		10800	S3
		10810	S3
		10815	S3
		10820	SS3
		10825	C
		10830	C
		10850	C
		10900	C
		10950	C
		11000	C
		11050	P4
		11060	C
		11065	All solutions evolve to steady branch

TABLE 2. Classification of numerical solutions of partial differential equations obtained for aspect ratio $\lambda = 1.5$, with $R_S = 10^4$, $\tau = 0.316$ and $\sigma = 1$
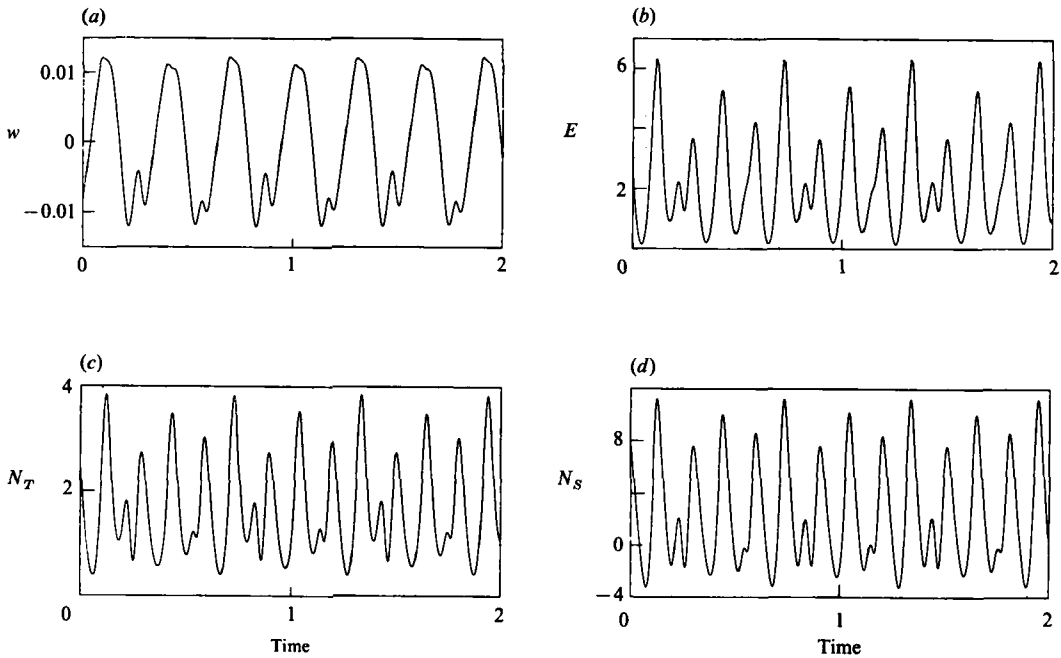
FIGURE 8. Time series for a period-4 solution on the first oscillatory branch ($R_T = 10050$). (a) Vertical velocity $w(0, \frac{1}{2}, t)$; (b) $E(t)$; (c) $N_T(\frac{1}{2}, t)$; (d) $N_S(\frac{1}{2}, t)$. The time series displays an overall period $P = 16\pi/\omega_0 = 1.2140$.

and apparently begins at $R_T \approx 10300$; for smaller R_T only the first branch exists (see figure 6). We now describe the bifurcations on the second branch, starting with the symmetrical period 1 (S1) solution at $R_T = 10300$ (figure 9a). We display, as in figure 7, the kinetic-energy phase plane and the energy power spectrum; comparing the $(E, \dot{E})$ trajectory here with that of the S1 solution on the first oscillatory branch in figure 7(a), we find that an additional distinguishing loop is now present. Moreover, the period P has increased from 0.338 (for the S1 solution at $R_T = 10500$) to 0.384. We also show in the bottom panels the Poincaré return map obtained by plotting the values of the Nusselt numbers N_T, N_S, evaluated at $z = \frac{1}{2}$, each time the vertical velocity $w(x = 0, z = \frac{1}{2}, t)$ passes through zero from negative to positive. For the S1 solution this procedure generates a single point.

As on the first branch S1 undergoes a bifurcation to asymmetry followed by a succession of period-doubling bifurcations as R_T is increased. In figure 9(b) we show a P4 solution present for $R_T = 10470$. The Poincaré map now has four points. These period-doubling bifurcations accumulate very rapidly. At $R_T = 10472$ we are already in the aperiodic regime and figure 9(c) shows the SP8 solution found there. Here the spectrum is noisy, but still contains peaks down to $\frac{1}{8}\omega_1$. The Poincaré map shows eight regions that are visited in regular order, although only four regions can be distinguished clearly. At $R_T = 10475$ in figure 9(d) the solution is probably SP2, and the Poincaré map has coalesced into a curve with a hook. At $R_T = 10485$ in figure 9(e), we have an SP1 solution whose Poincaré map looks distinctly different. As R_T is increased further we come to the first of our period 3 windows. The appearance of the window is heralded by intermittency associated with the saddle-node bifurcation that produces the periodic solution. Such an IS3 solution found at $R_T = 10508$ is
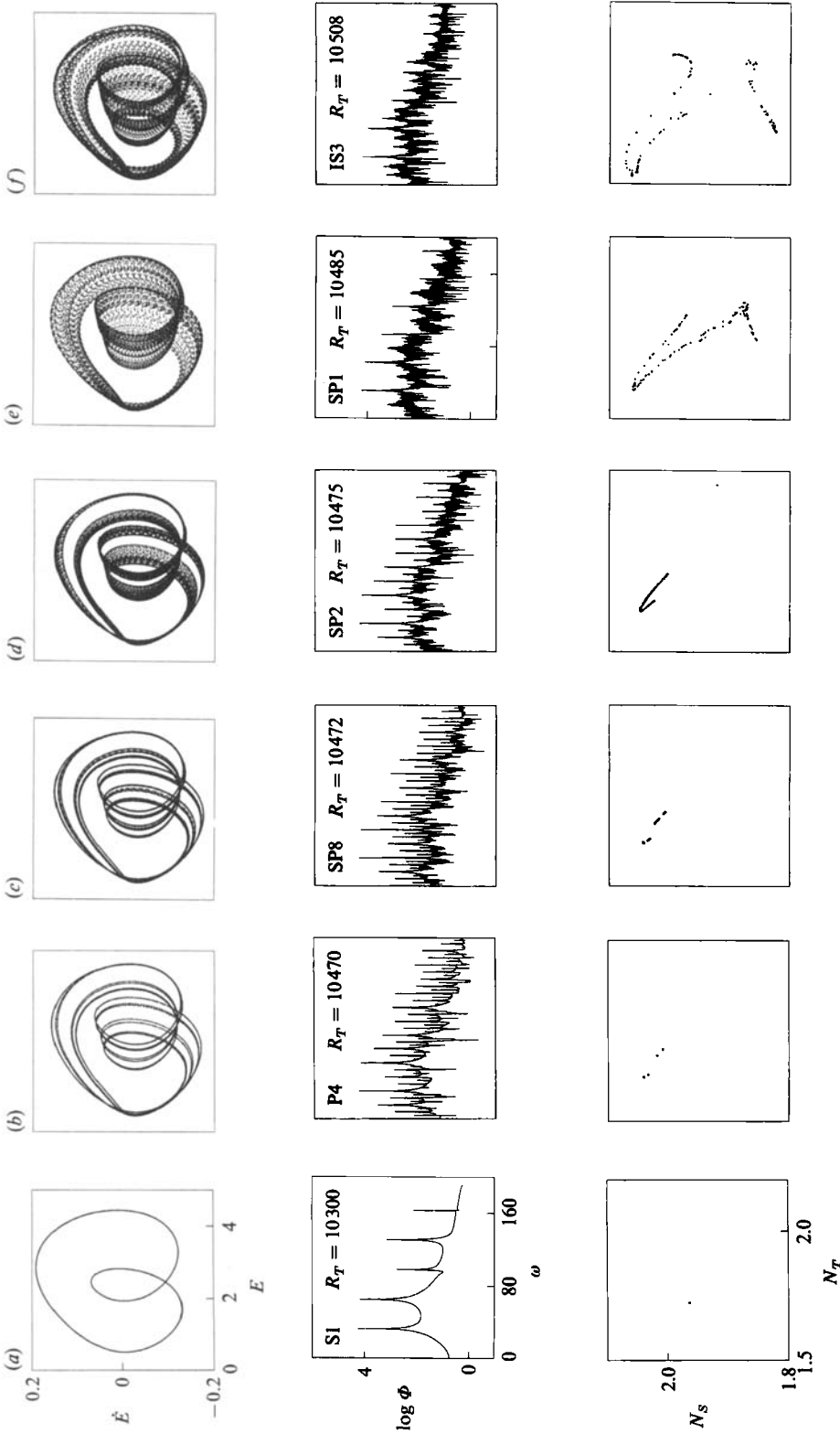
FIGURE 9. Solutions of the partial differential equations: the second oscillatory branch for $\lambda = 1.5$, $\sigma = 1.0$, $\tau = 0.316$, $R_S = 10^4$ and a succession of R_T values, with the solutions classified as indicated. In addition to the kinetic-energy phase plots $\dot{E}$–E and power spectra $\Phi(\omega)$ in the first and second rows, the third row shows the Poincaré return maps of N_T vs. N_S each time $w(0, \frac{1}{2}, t)$ crosses zero from negative to positive.
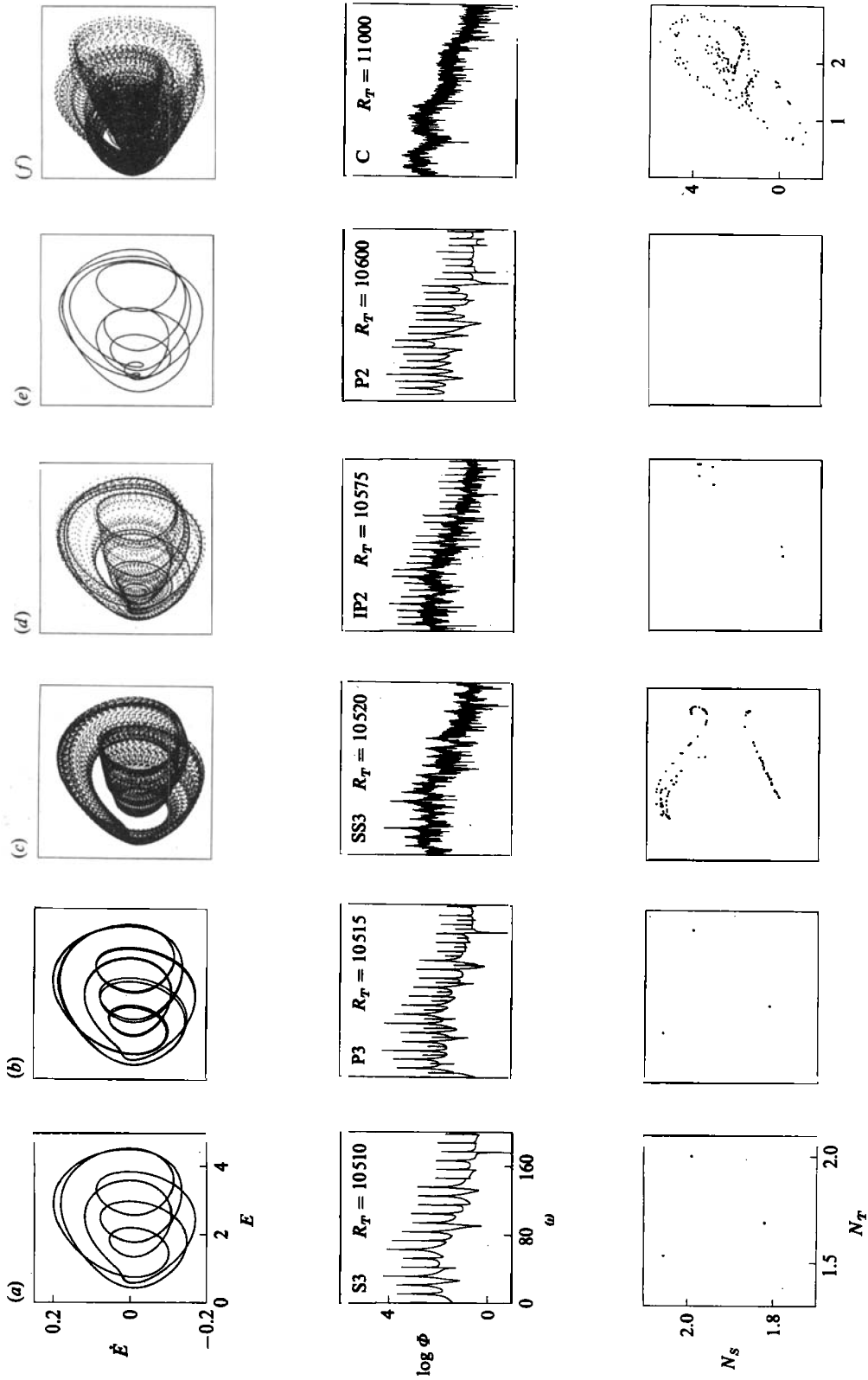
FIGURE 10. As for figure 9, but for a succession of higher values of R_T. Note the periodic window based on the symmetrical period-3 solution shown for $R_T = 10510$.

shown in figure 9 (f). This intermittent behaviour can just be detected in the spectrum and the Poincaré map.

In figure 10(a) we show a symmetric period 3 solution (S3) at $R_T = 10510$. It manifests itself by having peaks in the spectrum at ω_0, $\frac{2}{3}\omega_0$, and $\frac{1}{3}\omega_0$, along with various harmonics, while the Poincaré map has shrunk to just three points. This period 3 solution undergoes a bifurcation to asymmetry (P3) followed by period-doubling bifurcations producing P6, P12, and so on. We have found such solutions at $R_T = 10515$ (P3) shown in figure 10(b) and at $R_T = 10516$ (P6). These solutions have frequencies $\frac{1}{6}\omega_0$ and $\frac{1}{12}\omega_0$ in their spectra, respectively. These period-doubling bifurcations apparently accumulate rapidly leading to a semiperiodic regime based on period 3. At $R_T = 10517$ we have found an SP3 solution, and at $R_T = 10520$ in figure 10(c) there is a semiperiodic symmetrical solution of period 3 (SS3). As R_T is increased further the three peaks associated with the frequencies ω_0, $\frac{2}{3}\omega_0$ and $\frac{1}{3}\omega_0$ are gradually replaced by two peaks at ω_0 and $\frac{1}{2}\omega_0$ and their harmonics superposed on a noisy spectrum. Such an SP1 solution is found at $R_T = 10525$. At $R_T = 10575$ in figure 10(d) we find an intermittent period-2 solution (IP2), which gives way to a periodic solution of period 2 at $R_T = 10600$ in figure 10(e). Another period-3 window was located at $R_T = 10675$ (IS3), $R_T = 10700$ (P3), and after an interval of chaos again at $R_T = 10775$ (S3), $R_T = 10800$ (S3), $R_T = 10810$ (S3), $R_T = 10815$ (S3) and $R_T = 10820$ (SS3). It is likely (cf. Glendinning & Sparrow 1984) that these windows are on additional but coexisting oscillatory branches. Thereafter the solutions become increasingly chaotic (cf. figure 10f), although at $R_T = 11050$ we have found another P4 solution. The 'second' oscillatory branch finally terminates around $R_T \approx 11060$ and the solution evolves to a steady state.

In figure 11 we provide a different description of some of the aperiodic solutions shown above. The projection of the phase space motion onto the $u(x = \frac{3}{4}, z = 0, t)$ vs. $w(x = 0, z = \frac{1}{2}, t)$ plane shown in the top row, and the phase plots of the horizontal velocity $u(x = \frac{3}{4}, z = 0, t)$ shown in the second row, both provide new information about the oscillations. In the bottom row of panels we show the kinetic-energy return plots in which successive maxima of the kinetic energy are plotted against each other. Numerical artifacts in determining the maxima are eliminated by making the criterion for a maximum relatively coarse. In figure 11(a) we show our only example from the first oscillatory branch, the SP2 solution at $R_T = 10100$, with a double-banded structure. The remaining examples in figures 11(b)–(e) are all taken from the second branch: $R_T = 10475$ (SP2), $R_T = 10508$ (IS3), $R_T = 10625$ (C) and $R_T = 11000$ (C). We observe that as the degree of chaos increases with increasing R_T, so does the region in phase space visited by the trajectory. The gross features such as the approximate symmetry of the trajectory, and the spiralling motion around two symmetrically disposed points in phase space, remain unchanged. However, increasing R_T serves to broaden the structures in phase space, even though the impression of a folded ribbon is preserved. The return maps on the other hand show a much more dramatic evolution. We conjecture, by analogy with the fifth-order model (Da Costa *et al.* 1981, Knobloch & Weiss 1983), that the trajectory approaches the (generalized) saddle corresponding to the unstable steady solutions that bifurcate from R_T^e along its stable manifold and leaves again along the unstable manifold. A point describing the trajectory remains for a relatively long time near these two points in phase space.

The results for the second oscillatory branch are shown schematically in figure 6, while all our numerical solutions are classified in table 2. From this we conclude that we have traversed at least two bubbles on the second or subsequent branches while
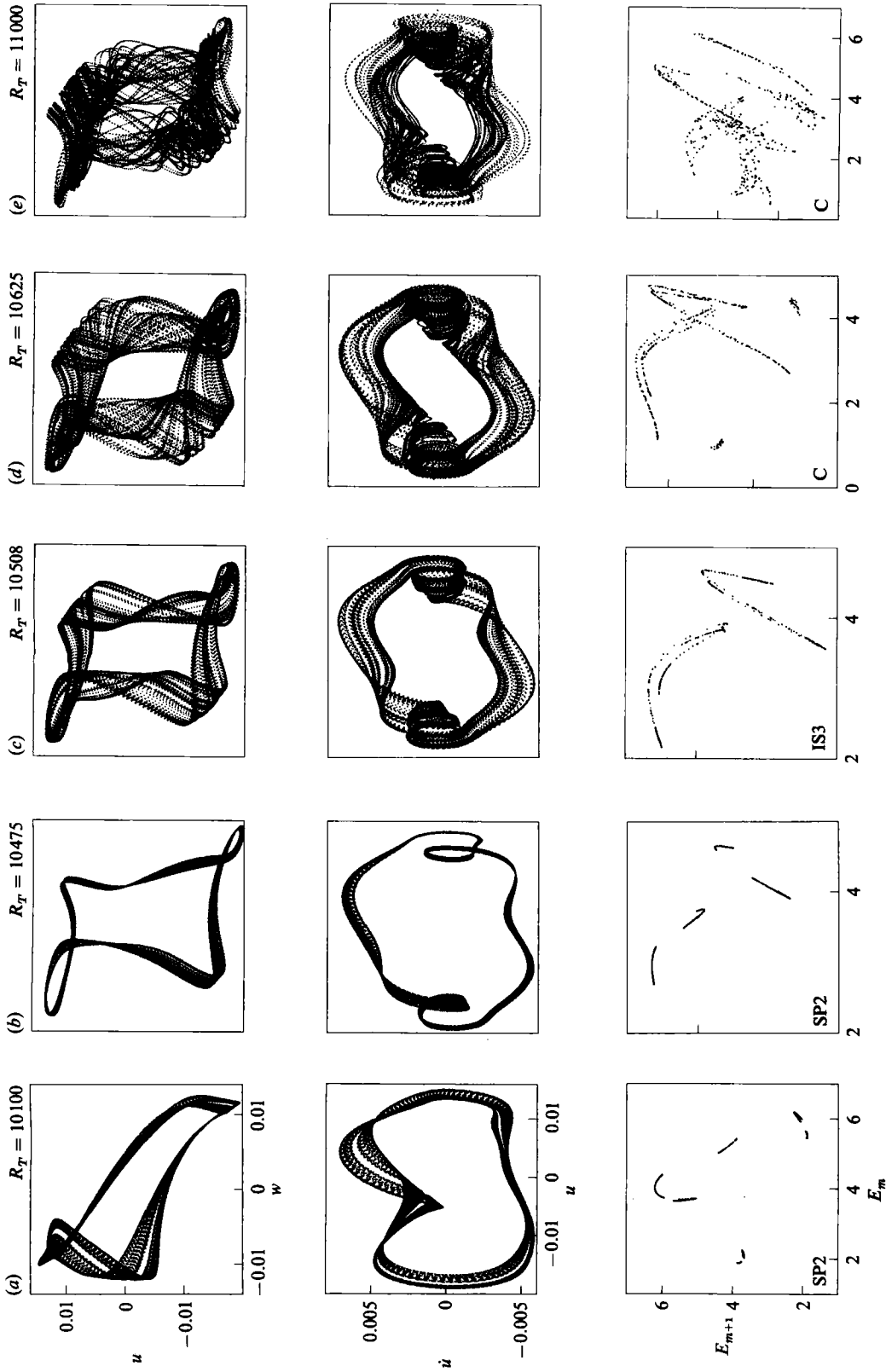
FIGURE 11. Different representations of chaotic solutions for $\lambda = 1.5$, $\sigma = 1.0$, $\tau = 0.316$ and $R_S = 10^4$. Top row: phase projection of $u(\frac{3}{4}, 0, t)$ *vs.* $w(0, \frac{1}{2}, t)$; second row: phase plots $\dot{u}(\frac{3}{4}, 0, t) - u(\frac{3}{4}, 0, t)$; third row: kinetic-energy return maps (successive maxima in $E(t)$ plotted against each other). Shown in (a) is a solution at $R_T = 10100$ on the first oscillatory branch and in (b) to (e) a succession of chaotic solutions on the second oscillatory branch. Note the spiral structure near the unstable steady solutions.
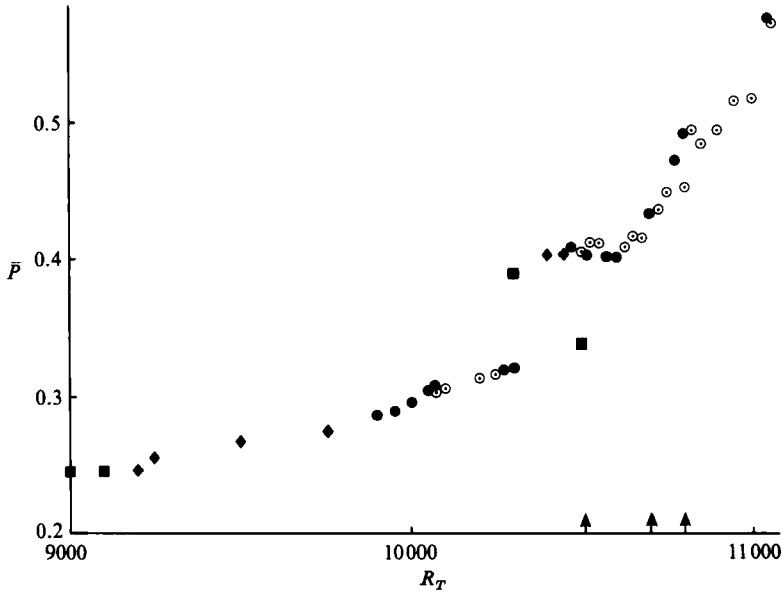
FIGURE 12. Solutions with $\tau = 0.316$ and $R_S = 10^4$. The mean cycle period $\bar{P}$ is plotted against R_T for most of the solutions in table 2. S1 solutions are denoted by squares, P1 solutions by diamonds and other periodic solutions by filled circles. Aperiodic solutions are shown by hollow circles. The arrows indicate three separate S3 windows.

increasing R_T, each with chaotic intervals and periodic windows. As can be seen from figures 7, 9 and 10, it is always easy to identify that non-zero value $\bar{\omega}$ of the frequency for which $\Phi(\omega)$ attains an absolute maximum. It is then possible to order the various solutions in terms of the mean cycle period, $\bar{P} = 4\pi/\bar{\omega}$. For a periodic solution, characterized as Sn or Pn, $\bar{\omega} = \omega_0$ and $\bar{P} = P/n$; for aperiodic solutions, $\bar{P}$ is a measure of the average cycle period. In figure 12 we plot $\bar{P}$ against R_T for the solutions discussed in this section, indicating various periodic solutions that have been obtained. This is a convenient way of summarizing our results. The distinction between the first and second oscillatory branches is apparent and it is clear that $\bar{P}$ increases rapidly towards the end. Periodic and chaotic solutions beyond the second oscillatory branch show considerable scatter but there is evidence for the presence of at least four bubbles in the diagram. These points clearly correspond to a more complicated bifurcation diagram than those obtained in figures 1 (*a*) and 2 (*a*). In the next subsection we explain how such behaviour is related to theoretical results.

3.4. *Origin of the complicated dynamics*

In this section we offer an explanation for the complex behaviour exhibited by solutions of the partial differential equations (1)–(3). This explanation depends on results which have only been proved for much simpler systems, and the extension to our problem relies on reasonable conjecture rather than on formal proof. It is, however, supported by numerical and analytical results for the fifth-order system (21)–(25). Moreover, it provides the only rationalization of our results that is currently available. There exist related problems for which it is possible to provide a more elaborate treatment. Thus Guckenheimer (1981) has rigorously analysed a reaction–diffusion system, while Arnéodo *et al.* (1985*a*) have derived normal form equations for a tricritical bifurcation in rotating thermosolutal convection. In what

follows we shall first consider the transition to chaos and the related bubble structure; then we shall indicate how the Shil'nikov mechanism leads to the formation of bubbles near a heteroclinic bifurcation.

3.4.1. *Bubbles and the transition to chaos*

For one-dimensional maps the period-doubling route to chaos is familiar and well understood (May 1976; Collet & Eckmann 1980; Holmes & Whitley 1984, and references therein.) Let $x \to f_\mu(x)$ be a non-invertible single-humped map of the unit interval into itself, depending on a bifurcation parameter μ. Then there is a universal period-doubling structure which occurs asymptotically at a geometric rate δ_F such that, if μ_N denotes the value of μ at which a bifurcation to a solution of period 2^N occurs, then

$$\delta_F = \lim_{N \to \infty} \frac{\mu_N - \mu_{N-1}}{\mu_{N+1} - \mu_N} \approx 4.669 \tag{30}$$

(Feigenbaum 1978). At the accumulation point μ_∞ there are aperiodic solutions; beyond it there are semiperiodic bands that merge pairwise as μ is increased further (Lorenz 1979). Thus the semiperiodic bands undergo a period-halving cascade which accumulates backwards at the same rate δ_F. It is punctuated by a succession of windows in μ within which there are periodic solutions. Each window is characterized by the periodicity of the basic solution; these periodic solutions are born in saddle-node bifurcations and their appearance is therefore heralded by intermittency (Pomeau & Manneville 1980). As μ is increased each basic periodicity undergoes its own period-doubling cascade leading to more aperiodic solutions. The sequence of new periodicities is given by Sharkovsky's (1964) ordering (Guckenheimer & Holmes 1983) and the order of actual appearance of the periodic windows, as well as the number of windows of each periodicity, has been established by Metropolis, Stein & Stein (1973).

This description can be extended to multi-dimensional maps (Collet, Eckmann & Koch 1981), but the tidy ordering of periodic windows disappears. Holmes & Whitley (1984) discuss two-dimensional maps of the form $(x, y) \to (y, -\epsilon x + f_\mu(y))$, which collapse into a one-dimensional map as $\epsilon \to 0$; the best-known example is the Hénon (1976) map, with $f_\mu(y) = \mu y(1-y)$, which is contracting for $0 \leqslant \epsilon < 1$ and collapses into the familiar logistic map as $\epsilon \to 0$. For finite ϵ the ordering of saddle-node bifurcations (which introduce the periodic windows) is upset so that, for example, the initial period-doubling sequence is interrupted by the window based on period 3 (Arnéodo *et al.* 1983); all that can be assured is that the canonical order is preserved for windows with low periodicities, provided ϵ is sufficiently small (Holmes 1984).

The universal period-doubling structure extends also to systems of ordinary differential equations (Feigenbaum 1980). In figure 13(*a*) the horizontal direction represents the space of all ordinary differential equations (of finite order) and the bifurcation parameter μ is plotted vertically. The horizontal surfaces, labelled PN, correspond to values μ_N at which the period of the solution of the corresponding differential equation doubles. Consider now a particular differential equation depending on a parameter such as R_T. As R_T is varied the differential equation varies too. Thus changes in R_T typically correspond to horizontal and vertical displacements in figure 13(*a*). If increasing R_T produces a path that crosses a certain number of bifurcation surfaces, then the differential equation will exhibit that number of period-doubling bifurcations. If $\mu(R_T)$ is double valued, then increasing R_T further results in a backward passage through the bifurcation sequence (cf. figure 13*a*) and
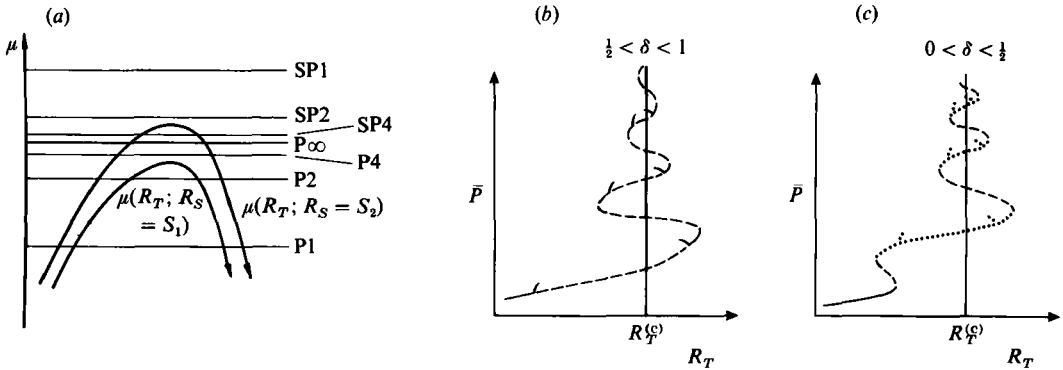
FIGURE 13. (a) Bifurcation structure in the space of functions. Horizontal lines are bifurcation surfaces, at which solutions appear as indicated. Curved lines indicate typical paths through this diagram as the parameter R_T is varied for different values of R_S. (b) Variation of normalized period, $\bar{P}$, with the bifurcation parameter, R_T, in the neighbourhood of a homoclinic bifurcation at $R_T^{(c)}$, when $\frac{1}{2} < \delta < 1$. (c) The same, when $0 < \delta < \frac{1}{2}$. Full, broken and dotted lines represent stable, non-stable and unstable solutions respectively. Successive branches meet at saddle-node bifurcations and bubbles are bounded by pitchfork bifurcations.

a bubble is formed. Now suppose that the system depends on a second parameter R_S. Then by varying R_S it may be possible to arrange that upon varying R_T (for fixed R_S) it is possible to penetrate deeper and deeper into the bifurcation set until chaotic behaviour is observed. This description allows us to explain the development of a single bubble in terms of a single-humped map f_μ. We could alternatively have introduced a double-humped map and the Shil'nikov mechanism (to be discussed below) corresponds to a many-humped map. Note, however, that our visualization of the abstract structure of the problem is quite general; thus R_T need not refer to a parameter (or a set of parameters) in a differential equation and could equally refer to changes in the differential equation arising for instance by the addition of new terms.

Beyond the accumulation point, labelled $P\infty$, lie semiperiodic bands, culminating with SP1. Superimposed upon this sequence is a similar pattern corresponding to every periodic window created by a saddle-node bifurcation. Although there is no *a priori* reason to expect a canonical ordering of these windows, numerical investigation of fifth-order systems suggests that the Sharkovsky ordering is followed, at least for low-period cycles in the first bubble (Knobloch & Weiss 1983). In the solutions described in §3.2 we could penetrate as far as the SP1 level on the first oscillatory branch but did not detect any periodic windows. The prominence of a window depends on its proximity to the vertex of the curve $\mu(R_T, R_S)$ in figure 13(a): if it occurs near the vertex the window will appear wide in R_T-space. By changing R_S, different windows can therefore be made prominent and easier to find.

Figure 13(a) has been drawn for equations possessing a symmetry which allows periodic solutions that are symmetrical in time. This temporal symmetry is given by (19) for the partial differential equations and by (27) for the fifth-order system. It is well-known that a symmetrical oscillation cannot undergo a period-doubling bifurcation (P. Swinnerton-Dyer 1980, private communication; Swift & Wiesenfeld 1984). If period-doubling occurred, the associated return map would have to have a single eigenvalue -1. The symmetry would then imply the existence of a return map with a single real eigenvalue λ such that $\lambda^2 = -1$, which is impossible.
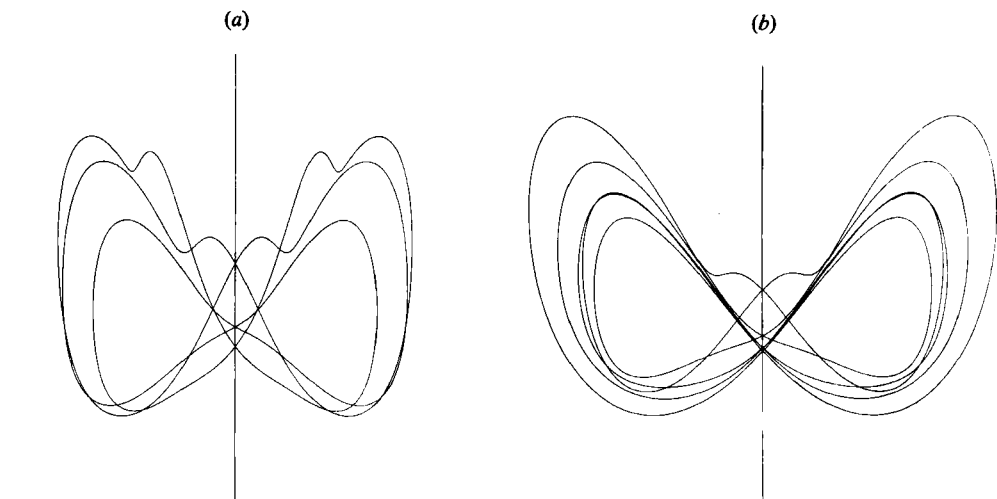
FIGURE 14. Symmetrical periodic solutions for partial differential equations with $\lambda = 1.414$, $\sigma = 1.0$. (a) S3 window for $\tau = 0.316$, $R_S = 10^4$ at $R_T = 10\,750$. (b) S5 window for $\tau = 0.1$, $R_S = 10^{3.5}$ at $R_T = 3674$. Orbits are projected onto the $(\langle u \rangle, N_T)$-plane.

Symmetrical solutions typically undergo a bifurcation that breaks the symmetry before indulging in a cascade of period-doubling bifurcations. In figure 13 (a) there is therefore a surface, labelled P1, corresponding to bifurcation to asymmetry. Similarly, the two asymmetrical semiperiodic bands finally merge to produce aperiodic solutions that are (statistically) symmetrical (Knobloch & Weiss 1983). Within this region there are windows based on cycles with odd periodicity; the last window to appear is that based on S3. Seeing this window implies that, if the system is sufficiently dissipative to be described by a one-dimensional map, there are windows with asymmetrical and symmetrical orbits of all possible periodicities at lower values of R_T. Since these windows can be exceedingly narrow, one should not expect to be able to locate them without special effort, if at all. Even in low-order systems this is a delicate task, and detailed study of a fifth-order model of magnetoconvection (Knobloch & Weiss 1983) reveals the complexity of the window structure and the difficulties in locating individual windows.

In our numerical results, the bifurcation to asymmetry leads to the appearance of a peak at $\omega_1 = \frac{1}{2}\omega_0$ (and its harmonics) in the power spectrum of the kinetic energy E. At each successive period-doubling bifurcation, new peaks appear at frequencies $\frac{1}{2}\omega_1, \frac{1}{4}\omega_1, \ldots$. We estimate that bifurcations to solutions P2, P4, P8 on the first oscillatory branch occur, respectively, at $R_T = 9900$, $10\,040$, $10\,068$ (cf. §3.2). Now the Feigenbaum constant δ_F can be found from the values of R_T at which successive bifurcations occur, since the slope $\partial\mu/\partial R_T$ factors out of equation (30) for N sufficiently large. (Note, however, that corrections to the Feigenbaum scaling do depend on the slope and are not universal.) From our results we estimate $\delta_F \approx 5.0$, with an error of some 20 % (cf. equation (30)).

Beyond the accumulation point the spectral peaks broaden; if the lowest frequency peak corresponds to a frequency $2^{-N}\omega_1$, we speak of a semiperiodic solution of period N. As R_T is increased this peak is submerged in the noise, leaving a solution of period $N-1$. Thus we are able to classify the aperiodic solutions in figures 7, 9 and 10. Although we have not searched systematically for periodic windows (such a search

is hardly practicable) we have found three symmetrical period-3 windows on the second and subsequent branches of figure 6. Figure 14(a) shows a symmetrical trajectory for $\lambda = 1.414$, projected onto the $(\langle u \rangle, N_T)$-plane, while figure 7 gives details of the window at $R_T \approx 10510$. Once again, the first bifurcation breaks the symmetry. The symmetrical orbit of figure 7(a) has peaks in the spectrum at $\frac{1}{3}\omega_1$ and $\frac{2}{3}\omega_1$, while the asymmetrical orbit of figure 7(b) has a peak at $\frac{1}{6}\omega_1$ and the P6 solution at $R_T = 10516$ has a peak at $\frac{1}{12}\omega_1$. The aperiodic SP3 solution at $R_T = 10517$ retains a peak at $\frac{1}{6}\omega_1$, which is submerged by noise in the SS3 spectrum at $R_T = 10520$, in figure 7(c). We have found no windows based on an asymmetrical period-3 orbit though we have located windows based on period 5, period 6 and period 9 in computations with $\tau = 0.1$. As indicated above, the ease with which a particular window is picked up depends on the curve $\mu(R_T)$; so it is not surprising that different windows are found in non-systematic studies at different values of the parameters τ and R_S.

3.4.2. *Homoclinic and heteroclinic bifurcations*

It remains to address the origin of the complex dynamics described in §§3.2–3.3. We shall argue that the chaotic dynamics and the repeated bubble structure are associated with the presence of a heteroclinic orbit, connecting a pair of saddle foci, in the partial differential equations (1)–(3). The importance of homoclinic (or heteroclinic) orbits was established by Shil'nikov (1965; see also Guckenheimer & Holmes 1983, Guckenheimer 1984) who considered a third-order system of ordinary differential equations containing a homoclinic orbit connecting a saddle focus to itself (see figure 4b). At the saddle focus there are three eigenvalues: one (s_1) is real and positive, while the others $(s_{2,3} = -\alpha \pm i\beta)$ form a complex-conjugate pair with negative real parts. Shil'nikov proved that, if a homoclinic orbit exists when a parameter $R_T = R_T^{(c)}$, such a system possesses complicated orbits in a neighbourhood of the homoclinic orbit whenever the three eigenvalues at $R_T^{(c)}$ satisfy the inequality

$$\delta \equiv \frac{\alpha}{s_1} < 1, \quad \beta \neq 0. \tag{31}$$

More specifically, he proved that the Poincaré return map associated with the homoclinic orbit contains a countably infinite number of Smale's horseshoes. Each horseshoe contains an invariant Cantor set with an uncountable number of aperiodic orbits and a countably infinite number of periodic orbits of arbitrarily long periods. It also contains a dense orbit, i.e. an orbit that comes arbitrarily close to each point of the invariant set. The orbits created are all non-stable since in any neighbourhood of such an orbit there is a non-recurrent orbit.

The practical implications of these statements have been clarified by recent work (Arnéodo, Coullet & Tresser 1982; Gaspard 1983; Glendinning & Sparrow 1984; Gaspard *et al.* 1984; Arnéodo *et al.* 1985b). For values of R_T near $R_T^{(c)}$ the local behaviour of orbits near the saddle focus is described by a two-dimensional map, whose fixed points correspond to periodic orbits. Their behaviour can be understood by plotting the period P against R_T for different values of δ (Glendinning & Sparrow 1984). For $\delta > 1$, P tends monotonically to infinity as $R_T \to R_T^{(c)}$, as indicated in figure 2(b). For $\delta < 1$ there is an extremely complicated set of bifurcations in which periodic orbits are created by saddle-node bifurcations and then undergo period-doubling cascades producing aperiodic orbits. When $\frac{1}{2} < \delta < 1$, $P(R_T)$ wiggles its way to infinity, as sketched in figure 13(b). The orbit first loses and then regains stability

at successive saddle-node bifurcations, and each complete wiggle corresponds to an extra loop around the singular point. As the orbit approaches homoclinicity, the period P therefore increases by $2\pi/\beta$ on successive stable branches, while the widths of the branches decrease rapidly, as $\exp(-2\pi\alpha/\beta)$. Furthermore, there is a bubble created by period-doubling bifurcations on each stable branch. Within this bubble other periodic orbits appear at pitchfork or saddle-node bifurcations and these orbits may themselves develop secondary homoclinicities, with structures similar to that in figure 13(b). When $0 < \delta < \frac{1}{2}$, the structure is as shown in figure 13(c). Now there are no stable orbits near homoclinicity, for the successive branches are alternately unstable or non-stable (as though the direction of time had been reversed). Such wiggles can only be joined to a stable periodic orbit through a pair of saddle-node bifurcations, as sketched in the figure.

In a system with a symmetry like (26), similar behaviour will be associated with heteroclinic orbits connecting a symmetrical pair of saddle foci. In the neighbourhood of a heteroclinic orbit satisfying the Shil'nikov inequality (31) we expect to see a highly complicated sequence of bifurcations, multiple attractors and complex time-dependent behaviour. Many of the periodic orbits will be stable (at least in narrow parameter ranges) and their period-doubling cascades, with the typical bubble structure, will be observable if $\frac{1}{2} < \delta < 1$. Explicit examples of such behaviour have been described by Sparrow (1982, chapter 8) and Glendinning & Sparrow (1984). Indeed, the predicted behaviour has been verified numerically for a fifth-order model of magnetoconvection (Knobloch & Weiss 1983; Bernoff 1985). In this system the bubbles are formed by symmetry-breaking bifurcations and the asymmetrical orbits may become homoclinic. One possible secondary homoclinic orbit is sketched in figure 4(b): the trajectory spirals in to only one of the saddle foci, unlike the heteroclinic orbit in figure 4(a), and the symmetry requires the existence of a companion orbit. Within a bubble secondary homoclinic or heteroclinic orbits can give rise to parameter intervals in which no stable orbits exist. Since to one side of such an orbit there are no stable orbits, a trajectory will leave this region of phase space and (in our case) spiral into the steady solutions present at larger amplitude, creating a gap in the oscillatory branch. Unless extreme care is taken, the appearance of a gap would then be interpreted as the termination of the oscillatory branch, although by carefully studying the morphology of the orbit it is (in principle) possible to determine at which secondary homoclinic orbit a transition is occurring (cf. Knobloch & Weiss 1983; Bernoff 1985).

For the fifth-order model described in §2.5 we know that there is a heteroclinic orbit for r_S close to $r_S^{(c)}$, connecting two real saddles, as shown in figure 1(b). For larger values of r_S the existence of such an orbit can be confirmed numerically. As r_S increases the eigenvalues along the unstable steady branch evolve in the manner described in §2.5. We can explain the presence of period-doubling cascades, bubbles and multiple oscillatory branches for $r_S = 15$ by computing the eigenvalues s_i ($i = 1, ..., 5$) along the unstable steady branch. Numerical calculations suggest that a heteroclinic orbit occurs at $r_T^{(c)} \approx 13.565$; for this value of r_T the eigenvalues are found to be

$$s_1 = 1.730, \quad s_{2,3} = -0.882 \pm 1.732i, \quad s_4 = -1.753, \quad s_5 = -4.039. \tag{32}$$

Since the real negative eigenvalues s_4, s_5 are significantly less than $\mathrm{Re}\, s_2$ we expect that the dynamics in the vicinity of the saddle foci is adequately described by a three-dimensional system with $\delta \approx 0.510$. The rest of the heteroclinic orbit may lie

in higher dimensions without affecting Shil'nikov's result. Indeed Shil'nikov (1970) extended his theorem to cover a $(2n+1)$-dimensional case in which, in addition to (31),

$$s_1 > 0 > \operatorname{Re} s_2 > \operatorname{Re} s_i \quad (i = 4, 6, \ldots, 2n). \tag{33}$$

where the eigenvalues s_i $(i = 4, \ldots, 2n)$ can be real without affecting the results. The complex dynamics present in the fifth-order system for $r_S = 15$ thus finds a natural explanation in terms of the Shil'nikov mechanism. Moreover, in cases with $\delta > 1$ (so that (31) is not satisfied) no complicated dynamics is found. This can be checked, for example, for $r_S = 1$ or for the solutions given by Da Costa *et al.* (1981).

If we regard the partial differential equations (1)–(3) as a large but finite set of coupled ordinary differential equations, Shil'nikov's (1970) theorem guarantees a complicated sequence of bifurcations, multiple attractors, etc., as R_T approaches $R_T^{(c)}$, the value for which a heteroclinic orbit is present in the system (1)–(3), provided that the three dominant eigenvalues on the branch of unstable steady solutions satisfy Shil'nikov's inequality (31) and the remaining eigenvalues satisfy (33). For R_S sufficiently close to $R_S^{(c)}$ those dominant eigenvalues are real and the existence of a heteroclinic orbit can be established analytically (Knobloch & Proctor 1981). Numerical calculations (cf. figure 2b) suggest its presence for larger values of R_S. We conjecture that the heteroclinic orbit persists but (by analogy with the fifth-order system) that for $R_S > 10^{3.5}$ the eigenvalues s_2, s_3 at $R_T^{(c)}$ form a complex-conjugate pair and both (31) and (33) are satisfied.

Inspection of our numerical solutions provides convincing evidence for a saddle focus. The S1 solution at $R_T = 10\,300$, in figure 9(a), loops once around the singular point, while the P2 solution at $R_T = 10\,600$, in figure 10(e), has developed extra loops. More and more loops appear in the chaotic solutions (see the second row of figure 11) and just before the end of the oscillatory branch there are aperiodic trajectories that describe up to five successive loops. We have not attempted to obtain unstable steady solutions of the system (1)–(3) nor is it feasible to compute their eigenvalues. However, the similarity between our numerical results in figure 12 and the behaviour sketched in figure 13(b) is sufficiently close to suggest that the leading eigenvalues satisfy (31), with $\frac{1}{2} < \delta < 1$.

In particular, we note the presence of a complete bubble on the first oscillatory branch, which is separated from the second branch by an interval corresponding to the rotation period about the focus. Owing to non-local effects the first two branches are apparently broadened and displaced to lower values of R_T. The second branch probably extends over the range $10\,300 \leqslant R_T \leqslant 10\,700$, without any obvious gaps. Above it lie fragments of several branches, which cannot be separated by $\bar{P}$ alone. We note, however, that there are three different S3 windows, apparently from different branches. There are also indications that windows based on saddle-node bifurcations are displaced from the bubbles to which they are related (as might be expected from two-dimensional maps). There are several examples of multiple solutions, e.g. at $R_T = 10\,800$, with a chaotic solution and an S3 orbit obtained from different initial conditions and apparently on different branches. (Of course, any chaotic solution might be a case of preturbulence, which would disappear if the equations were integrated for long enough. For partial differential equations we cannot compete with the two-dimensional map studied by Gambaudo & Tresser (1983), where transient chaos gave way to periodic behaviour after 1.5×10^6 iterations.)

The asymmetrical appearance of the points toward the right of figure 12 suggests

that there may be gaps (corresponding to subsidiary homoclinic orbits) or that δ may be close to unity. In the fifth-order system, with $\delta \approx 0.51$, we were unable to find any stable oscillatory solutions after the transition to chaos in the first bubble, perhaps because the system was approaching the situation in figure 13 (c). Conversely, in the fifth-order model of magnetoconvection, with $\delta \approx 0.95$, chaos was easily found though nothing more than the initial bifurcation to asymmetry has turned up for the relevant partial differential equations. We suspect that the latter have $\delta < \frac{1}{2}$ so that any complicated dynamics is unstable. These differences show the limitations of our truncated models.

4. Evolution of the oscillatory branch for $\tau = 0.1$

In this section we describe how the simple oscillatory branch illustrated in figure 2 (a) evolves into the complex structure represented in figure 6. Since it is impossible to explore a five-dimensional parameter space in any systematic way, Huppert & Moore (1976) set $\sigma = 1$ and $\lambda = 2^{\frac{1}{2}}$, and chose two values of τ: for $\tau = 0.1$ and $\tau = 0.316$ they investigated behaviour along the branch of oscillatory solutions as R_T was increased for four fixed values of R_S. Their results with $\tau = 0.316$ were discussed in §2.3: for $R_S = 10^3$ solutions remain periodic until the oscillatory branch terminates, apparently with a heteroclinic orbit; a bifurcation to asymmetry appears when $R_S = 10^{3.5}$ and all the structure discussed in §3 is present when $R_S = 10^4$. The development of the first bubble can be explained by reference to figure 13 (a). It is computationally more convenient to make runs with $\tau = 0.1$, since interesting behaviour occurs at somewhat lower values of R_T. A brief sampling of oscillatory solutions at $\tau = 0.1$ has also recently been reported by Chang *et al.* (1982), though with modified boundary conditions. Following Huppert & Moore, we set $\sigma = 1$, $\lambda = 2^{\frac{1}{2}}$, $\tau = 0.1$ and vary R_T for each of $R_S = 10^{2.5}$, 10^3 and $10^{3.5}$. Our new results provide a substantially more detailed description of bifurcations along the oscillatory branch. These results are summarized in table 3.

For $\tau = 0.1$, convection sets in as overstable oscillations for all $R_S > R_S^{(c)} \approx 14.6$. When R_S is only slightly greater than $R_S^{(c)}$ the oscillatory branch terminates with a heteroclinic orbit connecting the symmetrical pair of saddle points corresponding to unstable steady solutions (Knobloch & Proctor 1981) as explained in §2.2. As R_S is increased the saddle points change into saddle foci and trajectories spiral in towards the unstable fixed points (cf. §§2.5 and 3.4). If the Shil'nikov inequality (31) is satisfied at the saddle foci then we may expect to find chaotic behaviour.

The first set of runs was made with $R_S = 10^{2.5} \approx 316$. Then $R_T^{(o)} = 970$ and symmetrical, periodic oscillations were found for $1000 \leqslant R_T \leqslant 1200$. A bifurcation to asymmetry occurs at $R_T \approx 1225$, followed by a period-doubling at $R_T \approx 1258$. The period-doubling sequence reaches its accumulation point by $R_T \approx 1263$ and the oscillatory branch terminates at $R_T = 1265$, possibly on a subsidiary homoclinic orbit (cf. §3.4.2). For this value of R_T, therefore, there is apparently a single stable oscillatory branch, with a cascade of period-doubling bifurcations near its end.

The next set of runs was for $R_S = 10^3$; by this value there are two parts to the oscillatory branch, with a complete bubble on each part. The branch begins at $R_T^{(o)} = 1366$ and there is a bifurcation from symmetry to asymmetry at $R_T \approx 1850$, followed by a bifurcation to period 2 at $R_T \approx 1900$. Semiperiodic solutions are found for $1910 \leqslant R_T \leqslant 1925$, with bifurcations back to give period 4 at $R_T = 1930$, period 2 at $R_T = 1940$, asymmetrical orbits at $R_T = 1950$ and symmetry by $R_T = 1960$. Thus there is a complete bubble on the first oscillatory branch. The transition to a

$R_S = 10^{2.5}$	$R_S = 10^3$	$R_S = 10^{3.5}$
$R_T^{(o)} = 970$	$R_T^{(o)} = 1346$	$R_T^{(o)} = 2535$
$R_T = 1000$ S1	$R_T = 1700$ S1	$R_T = 3500$ P1
1050 S1	1750 S1	3600 P1
1100 S1	1775 S1	3620 P2
1150 S1	1800 S1	3630 P2
1200 S1	1850 P1	3640 P4
1225 P1	1875 P1	3650 SP2
1250 P1	1900 P2	3660 SP2
1255 P1	1910 SP	3670 C
1260 P2	1920 SP4	3673 C
1262 P4	1925 SP4	3674 S5
1265 †	1930 P4	3676 P5
	1940 P2	3677 P10
	1950 P1	3678 P10
	1960 S1	3679 SP10
	1975 S1	3680 SP10
	1978 P1	3690 C
	1980 P2	3700 C
	1982 SP4	3750 C
	1985 P2	3800 SP2
	1987 P9	3805 P4
	1990 †	3810 P2
		3820 P1
		3830 P1
		3840 P1
		3850 S1
		3870 S1
		3900 C
		3950 C
		4200 †

† Solutions evolve to steady branch.

TABLE 3. Classification of numerical solutions of partial differential equations obtained for aspect ratio $\lambda = 1.414$, with $\tau = 0.1$ and $\sigma = 1$

second oscillatory branch takes place unobtrusively around $R_T \approx 1975$ and is followed by bifurcations to asymmetry ($R_T = 1978$), P2 ($R_T = 1980$), SP4 ($R_T = 1982$) and back to P2 ($R_T = 1985$). At $R_T = 1987$ there is an asymmetrical solution with period 9 and by $R_T = 1990$ the oscillatory branch has terminated.

With $R_S = 10^{3.5} \approx 3162$ ($R_T^{(o)} = 2535$), the overall behaviour is similar to that described in §3. The bubble on the first oscillatory branch is well-developed, with bifurcations from asymmetrical P1 to P2 and back again at $R_T \approx 3620$, 3815 respectively and semiperiodic solutions in the range $3650 \leqslant R_T \leqslant 3800$. Within this range we have located a symmetrical period-5 (S5) window. Figure 14(b) shows a trajectory for $R_T = 3674$, projected onto the $(\langle u \rangle, N_S)$-plane. This is followed by a (slightly) asymmetrical P5 solution at $R_T = 3676$ and P10 at $R_T = 3677$. This is the only window that we have found on the first oscillatory branch; we conjecture that it is the last window for this value of R_S and is therefore sufficiently prominent to be detected (cf. §3.4.1).

We have also explored behaviour at $R_S = 10^4$ and $10^{4.5}$, when the Hopf bifurcations at $R_T^{(o)}$ are subcritical (Huppert & Moore 1976). The results are inconclusive, owing

to limited spatial resolution, but they suggest the appearance of a second Hopf bifurcation, so that trajectories lie on a two-torus (instead of a limit cycle) in phase space. We suspect that this is followed by frequency locking and a period-doubling cascade that leads to chaos. Such behaviour is familiar from other calculations (e.g. Jones, Weiss & Cattaneo 1985) as well as from experiments, notably those of Libchaber *et al.* (1982, 1983) on convection in mercury. More runs at higher resolution are needed before the bifurcation structure for $R_S \geqslant 10^4$ can be unambiguously determined.

5. Conclusions

Transitions from periodic to chaotic oscillations in thermosolutal convection were found by Huppert & Moore (1976), who appreciated their significance (Huppert 1976, 1977), but misinterpreted the bifurcation to asymmetry as a period-doubling bifurcation. We have conducted a more systematic investigation of these transitions and demonstrated that it takes place by a cascade of period-doubling bifurcations. As an aid to interpreting the complex dynamics of this full system we studied a truncated fifth-order model. The model is of limited validity but its bifurcation structure remains sufficiently close to that of the full problem for it to be used to explain the origin of the chaotic behaviour that is observed. As we have seen, the onset of chaos is apparently associated with homoclinic and heteroclinic bifurcations where the oscillatory branch meets the unstable portion of the steady branch.

Our study of different types of periodic, aperiodic and semiperiodic behaviour comprised about 200 runs with different values of R_T, R_S, τ and λ. This extensive survey has clarified a number of issues. First, we have established that the transition to chaos proceeds via a sequence of period-doubling bifurcations after a preliminary bifurcation to asymmetry, and that the first three period doublings are consistent with the presence of a Feigenbaum cascade. Beyond the accumulation point of this cascade we found semiperiodic solutions, with trajectories that wandered aperiodically within tubes enclosing the unstable periodic solutions. As the Rayleigh number was increased, the tubes coalesced and low-frequency peaks in the power spectrum were successively submerged in noise. Interspersed with these chaotic bands are a number of periodic windows, i.e. intervals of R_T values for which there are attracting periodic solutions, each of which forms part of a period-doubling sequence. We found examples with basic periods of 9, 5 and 3, of which the last appeared to be most prominent. In the most extreme regime in τ that we investigated, there were indications that the bifurcation pattern changed: the first bifurcation led to doubly periodic motion on a two-torus, followed by frequency locking and a sequence of period-doubling bifurcations. These last results, however, need to be confirmed by more accurate computations.

The bifurcation structure on the oscillatory branch is complicated by the presence of bubbles, with forward and backward cascades of bifurcations, and of hysteresis between the first and second oscillatory branches. We have argued that this behaviour, as well as the complex window structure, is to be expected as the parameter value at which the Shil'nikov bifurcation occurs (cf. §3.4) is approached. Indeed, it is likely that the behaviour is even more complex than our calculations have revealed (cf. Glendinning & Sparrow 1984).

Chaotic solutions have been found for many systems of partial differential equations. Holmes & Marsden (1981) have established the presence of a single horseshoe for an example arising in magnetoelasticity. The Shil'nikov mechanism

produces infinitely many horseshoes. Guckenheimer (1981) proves that it is present near a codimension-two bifurcation in a reaction–diffusion problem described by partial differential equations in one space dimension. The same mechanism is typically also found near codimension-three bifurcations in continuous systems (Arnéodo *et al.* 1985*b*), as has recently been demonstrated for thermosolutal convection in a rotating system (Arnéodo *et al.* 1985*a*; Arnéodo & Thual 1985). R. L. Sani (private communication) assures us that period doubling has been found in simulations of three-dimensional Rayleigh–Bénard convection with rigid boundaries (cf. Upson *et al.* 1981). In other studies of three-dimensional convection, whether by use of truncated modal equations (Toomre, Gough & Spiegel 1982) or with the full equations (Schubert & Straus 1982; McLaughlin & Orszag 1982; Curry *et al.* 1984) the mechanism of transition to chaos still remains unclear.

Period doubling has also been observed in several experiments on other continuous systems. These include experiments on interacting baroclinic waves (Hart 1984), and the Belousov–Zhabotinsky reaction–diffusion system (Simoyi, Wolf & Swinney 1982). In the convection experiments this route to chaos is found only when the system is constrained by lateral boundaries so that only a few rolls are present. With wider cells, chaos may appear immediately after the onset of convection so that the transition process cannot be identified. It seems that period doubling is a feature of systems whose dynamics is constrained so that only a few modes can be excited. In our problem, the stringent geometrical constraints of two-dimensionality and symmetry about roll centres, and the imposed boundary conditions, (8) and (9), force solutions of the partial differential equations to behave somewhat like those of the fifth-order model. We have yet to find out how robust the attractors described in this paper will prove to be when these constraints are relaxed. In particular, we may expect the behaviour to change and to become more complicated when the symmetry constraint is removed, or the boundary conditions are changed to allow sideways fluxes, or when three-dimensional disturbances are admitted. We expect that the solutions described here would then be unstable to wider classes of disturbances, which might themselves become chaotic. With such a plethora of instabilities it would be difficult (and perhaps pointless) to analyse the transition to chaos.

The system we have studied already provides a surprisingly rich range of behaviour. We have been able to recognize patterns of bifurcations that are common to a variety of problems in a fully nonlinear regime, though we are not yet able to offer a physical, rather than a mathematical, explanation for the transitions that we have observed. However, studies of simpler model systems do suggest that period-doubling cascades are a characteristic feature of problems where there is a balance between opposing forces that are out of phase, and a heteroclinic (or homoclinic) orbit exists at some value (possibly infinite) of a stability parameter (e.g. Lorenz 1963; Moore & Spiegel 1966; Baker *et al.* 1971; Marzec & Spiegel 1980; Knobloch & Weiss 1983; Glendinning & Sparrow 1984; Jones *et al.* 1985; Arnéodo *et al.* 1985*b*; Spiegel 1985).

In conclusion, we emphasize that transitions to temporal chaos for simple systems with limited numbers of spatial modes are only part of a much larger problem. Real fluid-dynamical systems have complex spatial structure and spatial interactions can lead to complicated patterns of behaviour. Indeed, Bretherton & Spiegel (1983) have shown that such interactions may lead to chaotic behaviour in thermosolutal convection when R_T is only marginally greater than $R_T^{(o)}$ and the horizontal domain is very wide. Studies like our own suggest that investigating transitions to chaos for

simple systems is a fruitful line of research but there is still a long way to go before such systems can be related to real turbulence, with its intrinsically rich and intermittent spatial structure.

REFERENCES

ARNÉODO, A., COULLET, P. H. & SPIEGEL, E. A. 1985*a* The dynamics of triple convection. *Geophys. Astrophys. Fluid Dyn.* **31**, 1–48.

ARNÉODO, A., COULLET, P. H., SPIEGEL, E. A. & TRESSER, C. 1985*b* Asymptotic chaos. *Physica* **14** D, 327–347.

ARNÉODO, A., COULLET, P. H. & TRESSER, C. 1982 Oscillators with chaotic behavior: An illustration of a theorem by Shil'nikov. *J. Stat. Phys.* **27**, 171–182.

ARNÉODO, A., COULLET, P. H., TRESSER, C., LIBCHABER, A., MAURER, J. & D'HUMIÉRES, D. 1983 On the observation of an uncompleted cascade in a Rayleigh–Bénard experiment. *Physica* **6** D, 385–392.

ARNÉODO, A. & THUAL, O. 1985 Direct numerical simulations of a triple convection problem versus normal form predictions. *Phys. Lett.* **109** A, 367–373.

ARNOL'D, V. I. 1977 Loss of stability of self-oscillations close to resonance and versal deformations of equivariant vector fields. *Funct. Anal. Appl.* **11**, 85–92.

ARNOL'D, V. I. 1983 *Geometrical Methods in the Theory of Ordinary Differential Equations.* Springer. (Russian version, Moscow 1978).

ARTER, W. 1983 Nonlinear convection in an imposed horizontal magnetic field. *Geophys. Astrophys. Fluid Dyn.* **25**, 259–292.

BAINES, P. G. & GILL, A. E. 1969 On thermohaline convection with linear gradients. *J. Fluid Mech.* **37**, 289–306.

BAKER, N. H., MOORE, D. W. & SPIEGEL, E. A. 1971 Aperiodic behaviour of a non-linear oscillator. *Q. J. Mech. Appl. Maths* **24**, 391–422.

BERNOFF, A. J. 1985 Heteroclinic and homoclinic orbits in a model of magnetoconvection. Preprint.

BRETHERTON, C. & SPIEGEL, E. A. 1983 Intermittency through modulational instability. *Phys. Lett.* **96** A, 152–156.

BUSSE, F. H. 1978 Nonlinear properties of thermal convection. *Rep. Prog. Phys.* **41**, 1929–1967.

CHANDRASEKHAR, S. 1961 *Hydrodynamic and Hydromagnetic Stability.* Clarendon.

CHANG, S.-M., KORPELA, S. A. & LEE, Y. 1982 Double diffusive convection in the diffusive regime. *Appl. Sci. Res.* **39**, 301–319.

COLLET, P. & ECKMANN, J.-P. 1980 *Iterated Maps of the Interval as Dynamical Systems.* Birkhäuser.

COLLET, P., ECKMANN, J.-P. & KOCH, H. 1981 Period doubling bifurcations for families of maps on R^n. *J. Stat. Phys.* **25**, 1–14.

COULLET, P., TRESSER, C. & ARNÉODO, A. 1980 Transition to turbulence for doubly periodic flows. *Phys. Lett.* **77** A, 327–331.

CURRY, J. H., HERRING, J. R., LONCARIC, J. & ORSZAG, S. A. 1984 Order and disorder in two- and three-dimensional Bénard convection. *J. Fluid Mech.* **147**, 1–38.

DA COSTA, L. N., KNOBLOCH, E. & WEISS, N. O. 1981 Oscillations in double-diffusive convection. *J. Fluid Mech.* **109**, 25–43.

ECKMANN, J.-P. 1981 Roads to turbulence in dissipative dynamical system. *Rev. Mod. Phys.* **53**, 643–654.

FEIGENBAUM, M. J. 1978 Quantitative universality for a class of nonlinear transformations. *J. Stat. Phys.* **19**, 25–52.

FEIGENBAUM, M. J. 1980 The transition to aperiodic behaviour in turbulent systems. *Commun. Math. Phys.* **77**, 65–86.

GAMBAUDO, J. M. & TRESSER, C. 1983 Some difficulties generated by small sinks in the numerical studies of dynamical systems. *Phys. Lett.* **94** A, 412–414.

GASPARD, P. 1983 Generation of a countable set of homoclinic flows through bifurcation. *Phys. Lett.* **97** A, 1–4.

GASPARD, P., KAPRAL, R. & NICOLIS, G. 1984 Bifurcation phenomena near homoclinic systems: a two parameter analysis. *J. Stat. Phys.* **35**, 697–727.

GIGLIO, M., MUSAZZI, S. & PERINI, U. 1981 Transition to chaotic behaviour via a reproducible sequence of period-doubling bifurcations. *Phys. Rev. Lett.* **47**, 243–246.

GLENDINNING, P. & SPARROW, C. 1984 Local and global behaviour near homoclinic orbits. *J. Stat. Phys.* **35**, 645–696.

GOLLUB, J. P. & BENSON, S. V. 1980 Many routes to turbulent convection. *J. Fluid Mech.* **100**, 449–470.

GOUGH, D. O. & TOOMRE, J. 1982 Single-mode theory of diffusive layers in thermohaline convection. *J. Fluid Mech.* **125**, 75–97.

GREBOGI, C., OTT, A. & YORKE, J. A. 1983 Are three-frequency quasiperiodic orbits to be expected in typical nonlinear dynamical systems? *Phys. Rev. Lett.* **51**, 339–342.

GREBOGI, C., OTT, A. & YORKE, J. A. 1985 Attractors on an N-torus: quasiperiodicity versus chaos. *Physica* **15** D, 354–373.

GUCKENHEIMER, J. 1981 On a codimension two bifurcation. In *Dynamical Systems and Turbulence* (ed. D. A. Rand & L.-S. Young), pp. 99–142. Lecture Notes in Mathematics, vol. 898. Springer.

GUCKENHEIMER, J. 1984 Multiple bifurcation problems of codimension two. *SIAM J. Math. Anal.* **15**, 1–49.

GUCKENHEIMER, J. & HOLMES, P. 1983 *Nonlinear Oscillations, Dynamical Systems and Bifurcations of Vector Fields*. Springer.

GUCKENHEIMER, J. & KNOBLOCH, E. 1983 Nonlinear convection in a rotating layer: amplitude expansions and normal forms. *Geophys. Astrophys. Fluid Dyn.* **23**, 247–272.

HART, J. E. 1984 Laboratory experiments on the transition to baroclinic chaos. In *Predictability of Fluid Motions* (ed. G. Holloway & B. J. West), pp. 369–375. American Institute of Physics Conference Proceedings, vol. 106. American Institute of Physics.

HÉNON, M. 1976 A two-dimensional mapping with a strange attractor. *Commun. Math. Phys.* **50**, 69–77.

HOLMES, P. 1984 Bifurcation sequences in horseshoe maps: infinitely many routes to chaos. *Phys. Let.* **104** A, 299–302.

HOLMES, P. & MARSDEN, J. 1981 A partial differential equation with infinitely many periodic orbits: chaotic oscillations of a forced beam. *Arch. Rat. Mech. Anal.* **76**, 135–165.

HOLMES, P. & WHITLEY, D. 1984 Bifurcations of one- and two-dimensional maps. *Phil. Trans. R. Soc. Lond.* A **311**, 43–102.

HUPPERT, H. E. 1976 Transitions in double-diffusive convection. *Nature* **263**, 20–22.

HUPPERT, H. E. 1977 Thermosolutal convection. In *Problems of Stellar Convection* (ed. E. A. Spiegel & J.-P. Zahn), pp. 239–254. Lecture Notes in Physics, vol. 71. Springer.

HUPPERT, H. E. & LINDEN, P. F. 1979 On heating a stable salinity gradient from below. *J. Fluid Mech.* **95**, 431–464.

HUPPERT, H. E. & MOORE, D. R. 1976 Nonlinear double-diffusive convection. *J. Fluid Mech.* **78**, 821–854.

HUPPERT, H. E. & TURNER, J. S. 1981 Double-diffusive convection. *J. Fluid Mech.* **106**, 299–329.

JONES, C. A., WEISS, N. O. & CATTANEO, F. 1985 Nonlinear dynamos: a complex generalization of the Lorenz equations. *Physica* **14** D, 161–176.

KNOBLOCH, E. 1980 Convection in binary fluids. *Phys. Fluids* **23**, 1918–1920.

KNOBLOCH, E. & PROCTOR, M. R. E. 1981 Nonlinear periodic convection in double-diffusive systems. *J. Fluid Mech.* **108**, 291–316.

KNOBLOCH, E. & WEISS, N. O. 1981 Bifurcations in a model of double-diffusive convection. *Phys. Lett.* **85** A, 127–130.

KNOBLOCH, E. & WEISS, N. O. 1983 Bifurcations in a model of magnetoconvection. *Physica* **9** D, 379–407.

LANFORD, O. E. 1982 The strange attractor theory of turbulence. *Ann. Rev. Fluid Mech.* **14**, 347–364.

LIBCHABER, A., FAUVE, S. & LAROCHE, C. 1983 Two-parameter study of the routes to chaos. *Physica* **7** D, 73–84.

LIBCHABER, A., LAROCHE, C. & FAUVE, S. 1982 Period doubling cascade in mercury, a quantitative measurement. *J. de Physique-Lettres* **43**, L211–216.

LIBCHABER, A. & MAURER, J. 1981 A Rayleigh–Bénard experiment: helium in a small box. In *Nonlinear Phenomena at Phase Transitions and Instabilities* (ed. T. Riste), pp. 259–286. Plenum.

LORENZ, E. N. 1963 Deterministic nonperiodic flow. *J. Atmos. Sci.* **20**, 130–141.

LORENZ, E. N. 1979 On the prevalence of aperiodicity in simple systems. In *Global Analysis* (ed. M. Grmela & J. E. Marsden), pp. 53–75. Lecture Notes in Mathematics, vol. 755. Springer.

McLAUGHLIN, J. B. & ORSZAG, S. A. 1982 Transition from periodic to chaotic thermal convection. *J. Fluid Mech.* **122**, 123–142.

MARZEC, C. J. & SPIEGEL, E. A. 1980 Ordinary differential equations with strange attractors. *SIAM J. Appl. Math.* **38**, 403–421.

MAY, R. M. 1976 Simple mathematical models with very complicated dynamics. *Nature*, **261**, 459–467.

METROPOLIS, N., STEIN, M. L. & STEIN, P. R. 1973 On finite limit sets for transformations on the unit interval. *J. Comb. Theor.* **15** A, 25–44.

MOORE, D. R. 1985 Efficient explicit real FFTs for rapid elliptic solvers. *J. Comp. Phys.* submitted.

MOORE, D. R., PECKOVER, R. S. & WEISS, N. O. 1974 Difference methods for time-dependent two-dimensional convection. *Comp. Phys. Commun.* **6**, 198–220.

MOORE, D. R., TOOMRE, J., KNOBLOCH, E. & WEISS, N. O. 1983 Period-doubling and chaos in partial differential equations for thermosolutal convection. *Nature* **303**, 663–667.

MOORE, D. R. & WALLCRAFT, A. J. 1986 Rapid elliptic solvers for vector computers. In preparation.

MOORE, D. W. & SPIEGEL, E. A. 1966 A thermally excited non-linear oscillator. *Astrophys. J.* **143**, 871–887.

NEWHOUSE, S., RUELLE, D. & TAKENS, F. 1978 Occurrence of strange axiom A attractors near quasiperiodic flows on T^m, $m \geqslant 3$. *Commun. Math. Phys.* **64**, 35–40.

POMEAU, Y. & MANNEVILLE, P. 1980 Intermittent transition to turbulence in dissipative dynamical systems. *Commun. Math. Phys.* **74**, 189–197.

PROCTOR, M. R. E. & WEISS, N. O. 1982 Magnetoconvection. *Rep. Prog. Phys.* **45**, 1317–1379.

RUELLE, D. & TAKENS, F. 1971 On the nature of turbulence. *Commun. Math. Phys.* **20**, 167–192.

SCHECHTER, R. S., VELARDE, M. G. & PLATTEN, J. K. 1974 The two-component Bénard problem. In *Advances in Chemical Physics*, vol. 26 (ed. I. Prigogine & S. A. Rice), pp. 265–301. Interscience.

SCHUBERT, G. & STRAUS, J. M. 1982 Transitions in time-dependent thermal convection in fluid-saturated porous media. *J. Fluid Mech.* **121**, 301–313.

SHARKOVSKY, A. N. 1964 Coexistence of the cycles of a continuous mapping of the line into itself. *Ukr. Math. J.* **16**, 61–71.

SHIL'NIKOV, L. P. 1965 A case of the existence of a countable number of periodic motions. *Sov. Math. Dokl.* **6**, 163–166.

SHIL'NIKOV, L. P. 1970 A contribution to the problem of the structure of an extended neighbourhood of a rough equilibrium state of saddle-focus type. *Math. USSR Sbornik* **10**, 91–102.

SHIRTCLIFFE, T. G. L. 1967 Thermosolutal convection: observation of an overstable mode. *Nature* **213**, 489–490.

SHIRTCLIFFE, T. G. L. 1969 An experimental investigation of thermosolutal convection at marginal stability. *J. Fluid Mech.* **35**, 677–688.

SIMOYI, R. H., WOLF, A. & SWINNEY, H. L. 1982 One-dimensional dynamics in a multicomponent chemical reaction. *Phys. Rev. Lett.* **49**, 245–248.

SPARROW, C. T. 1982 *The Lorenz equations: Bifurcations, Chaos and Strange Attractors.* Springer.

SPIEGEL, E. A. 1985 Cosmic arrhythmias. In *Chaos in Astrophysics* (ed. R. Buchler, J. Perdang & E. A. Spiegel), pp. 91–135. Reidel.

STERN, M. E. 1960 The 'salt-fountain' and thermohaline convection. *Tellus* **12**, 172–175.

SWIFT, J. W. & WIESENFELD, K. 1984 Suppression of period doubling in symmetric systems. *Phys. Rev. Lett.* **52**, 705–708.

TAVAKOL, R. K. & TWORKOWSKI, A. S. 1984a On the occurrence of quasiperiodic motion on three tori. *Phys. Lett.* **100** A, 65–67.

TAVAKOL, R. K. & TWORKOWSKI, A. S. 1984b An example of quasiperiodic motion on T^4. *Phys. Lett.* **100** A, 273–276.

TOOMRE, J., GOUGH, D. O. & SPIEGEL, E. A. 1982 Time-dependent solutions of multimode convection equations. *J. Fluid Mech.* **125**, 99–122.

TURNER, J. S. 1968 The behaviour of a stable salinity gradient heated from below. *J. Fluid Mech.* **33**, 183–200.

TURNER, J. S. 1973 *Buoyancy Effects in Fluids.* Cambridge University Press.

UPSON, C. D., GRESHO, P. M., SANI, R. L., CHAN, S. T. & LEE, R. L. 1981 A thermal convection simulation in three dimensions by a modified finite element method. Preprint.

VERONIS, G. 1965 On finite amplitude instability in thermohaline convection. *J. Mar. Res.* **23**, 1–17.

VERONIS, G. 1968 Effect of a stabilizing gradient of solute on thermal convection. *J. Fluid Mech.* **34**, 315–336.